

Multiscale modelling of irradiation in nanostructures

Kai Nordlund · Flyura Djurabekova

Received: date / Accepted: date

Abstract Ion and electron irradiation can be used to modify not only conventional materials such as silicon, but also nanostructures. This opens up exciting possibilities for basic science studies of how materials behave under an external force driving them off equilibrium, and creating new kinds of nanostructures of potential application interest. Radiation effects are almost without exception a multiscale phenomenon, and hence modelling them theoretically requires the use of multiple different levels of simulation tools. In this Article we discuss the multiscale modelling framework relevant for modelling nanoscale phenomena, review briefly the most widely used modelling tools relevant for them, and present some recent examples of their use.

Keywords Multiscale modelling · Nanostructures · Radiation

1 Introduction

Particles with kinetic energies clearly above conventional thermal energies, i.e. with $E_{kin} > 1$ eV, exist in nature due to cosmic radiation and radiation decay. Nowadays such ions are also produced in a wide range of man-made devices for basic research and practical applications. For instance, the great accelerators at CERN and other particle physics laboratories in the world attempt to unravel the fundamental nature of the universe [1,2] and numerous smaller devices are

K. Nordlund
Department of Physics, PB 43, 00014 University of Helsinki, Finland
Tel.: +358-9-19150007
Fax: +358-9-19150042
E-mail: kai.nordlund@helsinki.fi

F. Djurabekova
Helsinki Institute of Physics and Department of Physics, PB 43, 00014 University of Helsinki, Finland

widely used for equally exciting research in physics [3], chemistry [4], medicine [5] and nanoscience [6]. On the application side, ion implantation is one of the key technologies in silicon chip manufacturing [7,8], and electron accelerators are having an important role in treating cancer [9]. All of these activities make it interesting and important to understand what the fundamental effects of high-energy particles on matter are.

Ion and electron irradiation can be used to modify along with conventional materials such as silicon also structures reduced to the nanosize, which are highly promising for future applications. Naturally, nanostructures are also relevant to current and future silicon technology (as also evidenced by the other articles in this Volume). In advanced transistor structures such as Fin-FET's [10], some of the active parts are spatially confined in two dimensions, which is the definition of a nanowire. In nanocluster memories [11] the key component is a quantum dot that is on the nanoscale in all dimensions. Small nanoclusters embedded in a silicon-based matrix [12] have exhibited new optical features, which may help to create a desirable combination of photonic and electronic devices in a single silicon chip [13–15]. On the other hand, ion implantation remains a key technology in semiconductor manufacturing [8]. The shrinking feature size, on the other hand, also increases the risk that natural radiation (from e.g. cosmic rays and radioactive isotopes) causes problems in transistor operation either in the form of single-event electronic upset events or long-term damage buildup. Both reasons make study of radiation effects in nanostructures of major interest for semiconductor technology.

Radiation effects are with a few exceptions a multiscale phenomenon, either in space or time, and usually in both. The exceptions include, for instance *low-energy, low-fluence, low-flux, low-temperature* sputtering yields may be determined fully by what happens in single cascades of nuclear collisions on nanometer length scales and picosecond time scales [16,17]. If the *ion energies* are not low but in the MeV regime, sputtering by electronic excitations may become dominant, making the effect multiphysics and thus multiscale, as the origin of sputtering and its later stages are described by different physical phenomena (electronic excitations and atomic motion), which also develop on the time scales different by several orders of magnitude [18–20]. If the *fluences* are not low, preferential sputtering will modify the surface composition, bringing in the necessity of applying a multiscale approach in describing the phenomenon since the physics and chemistry of materials composition change has to be included in understanding the sputtering yields [21–23]. If the *fluxes* are not low, which often is the case e.g during plasma bombardment of the materials, buildup of metastable surface layers [24] or overlapping of heat spikes [25] may strongly modify the sputtering yields, making the sputtering a multiphysics effect between materials and plasma physics. If the *temperatures* are not low, thermally enhanced desorption can enhance the sputtering yields dramatically, making the process multiscale in time [26,27].

Many other radiation effects are essentially always multiscale. The radiation damage production in almost any material practically always involves several stages, such as athermal primary damage production, thermally acti-

vated defect migration, phase changes and damage buildup. Fig.1 a illustrates the difference of time spans relevant to different physical processes. These processes can be combined in one to follow the irradiation process in total, including the possible long term consequences. Each of these processes traditionally are modelled by using simulation tools valid within the corresponding time spans. Due to the multiscale and multiphysics nature of radiation effects, it is natural that modelling the radiation effects theoretically requires the use of multiple different levels of simulation tools that are capable of handling different levels of physics. Fig.1b illustrates the simulation tools used to simulate different processes versus the time spans, within which the corresponding tool is valid.

The nanoscale is of special interest with respect to studying radiation effects. Nowadays there are several experimental tools (such as transmission electron microscopy (TEM) [28] and the scanning probe microscopies (SPM) [29–31], that are capable to image the nanoscale structures and features. These make it possible the direct study of primary damage created by ion irradiation, as this damage usually does not exceed the nanoscale. (several examples will be given later in this Article). This simplifies the use of multiscale modelling, in that the methods needed to achieve the macroscopic scale (right part of Fig. 1), such as finite-element modelling, might not be needed in nanoscale systems. This is of major basic science interest, as it reduces the level of complexity involved and hence may enable detailed direct study of fundamental radiation effects. Unfortunately the multiscale nature of modelling time still remains, as the time resolution of the common nanoscale experimental tools still remains of the order of magnitude of seconds (typical *in situ* TEM's have time resolutions of a normal video frame rate of 1/24 seconds, while SPM operation is often on the time scale of minutes.

Multiscale modelling is one of the concepts in current computational sciences to approach the problem of time and length span differences between simulations and experiments. It can be defined as using several different kinds of simulation models to address a physical question. Use of multiscale modelling is of course not limited to materials and nanoscience: for instance modelling of fusion plasmas regularly uses several different levels of plasma simulation methods [32]. In this Article, however, we restrict the discussion to materials science modelling.

Multiscale modelling methods can quite generally be divided into sequential and concurrent multiscale methods. Sequential multiscale modelling means that each physics model (and hence simulation code) is run separately from each other, and only a set of data is passed from one code to the next. A relatively simple example could be to use density-functional theory (DFT) calculations to obtain the migration prefactor and activation energy of points defects, and subsequently use these as the migration parameters in a separate kinetic Monte Carlo (KMC) simulation.

In concurrent multiscale modelling two or more physics models are run in the same simulation software, switching between the two models within

some simulation loop of the software, or even running them in parallel on a multiprocessor system.

Presently, multiscale modelling is much more often carried out sequentially rather than concurrently. The reason is in part simplicity in implementation, as making a tightly linked code with several different physics levels is certainly more difficult than implementing a single code. However, in many cases implementing a concurrent model would, even if theoretically possible, be completely impractical. To return to the DFT+KMC example on defect migration: in an alloy it could be beneficial to get the migration rates on the fly, as there is in principle an infinite number of migration rates when the atomic composition around a defect changes. However, as a DFT calculation of a single migration rate typically takes of the order of a day of CPU time, and a typical KMC calculation requires billions of steps, a concurrent DFT+KMC model would (while in principle relatively simple to implement) be prohibitively expensive computationally.

Naturally the distinction of sequential and concurrent multiscale modelling is not sharp. For instance, a situation similar to the DFT+KMC example can be handled by using DFT to parametrise a large number of migration energies for different defect configurations, then use either a parametrised equation [33] or artificial intelligence (AI) [34] to efficiently determine the migration energies within the KMC model. The latter approach can be classified as a hybrid sequential concurrent multiscale model, as it involves 3 different simulation models, two of which are run concurrently. Such a model allows within KMC runs for the barriers obtained on-fly by AI, but based on the initial information obtained by DFT or molecular dynamics (MD) methods prior the KMC simulation [34].

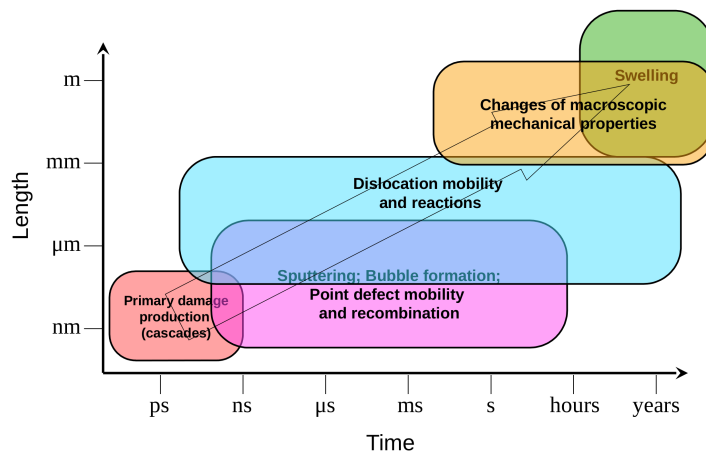
In this Article we discuss the multiscale modelling methods relevant for modelling nanoscale phenomena. The focus is on presenting the main principles of the most widely used tools relevant for modelling nanoscale radiation phenomena, and to present some recent examples of their use. The examples are chosen with emphasis on cases which are in some way, sequentially or concurrently, multiscale, and presented in order of the “highest-level” (time- or spacewise) simulation method description. This review does not attempt to be comprehensive, but rather to give a flavour of what can be done with present-day algorithms and computers. For more comprehensive reviews of radiation of nanostructures the reader is encouraged to consult other recent review articles, e.g. [35, 36, 6, 37].

In the next subsection, we give a brief overview of radiation physics. After this we proceed to discuss the methods and give selected examples of the use of each.

1.1 Overview of radiation physics

A charged particle traversing in matter is slowed down by energy loss to electronic excitations (electronic stopping power) and in collisions with atom

a)



b)

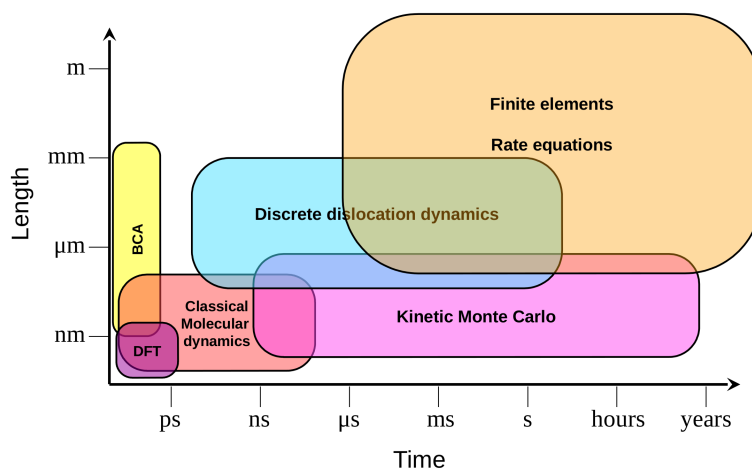


Fig. 1 Schematic of multiscale physics (top) and modelling (bottom) of radiation effects in materials. The boxes illustrate roughly the most appropriate usage range for the methods. The box limits should not, however, be understood very strictly, as they have been drawn not to overlap too much for clarity. For instance, finite-elements methods can be used down to the nm scale, and kinetic Monte Carlo for rapid processes well be sometimes used down to ps timescales. Naturally, for nanoscale objects, the physics and modelling methods for μm and larger scales is not necessarily relevant.

cores/nuclei (nuclear stopping power) [38,39,3]. The electronic excitations can cause damage in ionic materials or for very high ($> \text{MeV/amu}$) ion energies [40,41] in the so called swift heavy ion regime (see section 5.2.2). Photon irradiation creates damage largely by electronic excitation processes causing bond breaking [42], although very high-energy gamma photons can also produce damage by atomic recoil processes [43]. Neutrons create damage via several different mechanisms, but usually the most significant is giving lattice atoms a nuclear recoil energy in the 10 – 100 keV energy range [44].

The mechanisms by which the collisions with nuclei (primary knock-on atoms (PKA) from ions, neutrons or electrons) produce damage in a material can in most cases be well divided into two categories by time scale, see Fig. 2. The PKA induces a cascade of atomic collision processes and strong off-equilibrium material heating caused by the thermalization of the atoms. Numerous computer simulation and experimental studies have shown that the time scale for the ballistic atom collision processes is of the order of 100 fs, and the time scale for subsequent thermalization of the collisions 1 – 10 ps [45,46], see Fig. 2. After this athermal (meaning that equilibrium thermally activated processes are not significant) stage, long-time scale (nanoseconds to years) damage evolution caused by thermally activated processes can occur.

The first stage involves a dramatic and very quick change in energy of the system, while the latter stage involves numerous smaller and slower changes. Hence, the analogy with the flow of water in the original meaning of the word “cascade” (meaning a waterfall) could be logically extended to call the latter defect evolution stage a “defect rapids”. The word rapids is well motivated as most of the evolution occurs on subsecond timescales, which are very fast considered from a macroscopic human perspective.

The damage can take many forms: in a crystal it is easy to understand that an atom, if given sufficient energy, is kicked out from its initial lattice site, leaving an empty site (a vacancy) behind and creating an atom at an interstitial site in front [47]. It is important to appreciate that the formed crystal defects can also be much more complicated: they can, for instance, be defect clusters [48], amorphous zones [49], dislocation loops [50] or three-dimensional defects [51,52]. On surfaces, the damage can also take the form of adatoms [53], craters [54,55] and ripples [56,57], and in amorphous materials over- or undercoordinated atoms [58] or empty (porous) regions [59].

All defects are in principle mobile, as they are per definition in higher energy states than the ground energy state of atoms in the system [60] and there must be some energy barrier which, if overcome, would bring the atoms from the defect state back to the ground state. However, some mobility energies may be so high that the defect system becomes immobile and stops evolving for all practical purposes at a fixed temperature. For instance, in Si the single vacancy and interstitial defects are mobile [61], but some larger defects like e.g. the rod-like defects lying on 311 crystal planes (“311 defects”) [62,63] are essentially fully stable at room temperature. Similarly, in Cu it has been well established that larger vacancy clusters are fully stable at room temperature, but can be annealed out at elevated temperatures [64].

On the nanoscale, the above picture largely still holds, but the large surface-to-volume ratio characteristic of nanoobjects makes it more likely that surface or interface effects play a role, see illustration in Fig. 3. Numerous experiments and simulations show that the presence of a surface near a collision cascade can have major effects on the outcome [65–69, 54, 70–73, 55, 74, 56, 75, 53, 57]. Hence it is natural to expect that radiation effects in a nanostructure (which have surfaces in 2, 4 or 6 directions for nanofilms, nanowires and nanoparticles, respectively) can be profoundly different from those in the bulk.

In the following we give a short overview of different methods that are used to simulate radiation effects in nanostructures together with some examples of their application, which indeed in many cases demonstrate major differences to the behaviour in bulk systems.

2 Time-dependent Density Functional Theory

2.1 Method

Time-dependent density functional theory attempts to describe both atomic motion and electronic excitations in a system. It tries in principle to solve the time-dependent Schrödinger equation for all atoms and electrons in a system, but for computational efficiency, the real solution is replaced by the approximations of density-functional theory (see section 3 below).

It is computationally extremely demanding, and the algorithms are still strongly under development [76–79]. Practical TDDFT simulations seldom involve more than ~ 50 atoms and sub-picosecond timescales. However, the major advances in computational capacity coupled with TDDFT implementations in widely used codes such as SIESTA [80] have now started to make the use of TDDFT viable to study some aspects of radiation effects. TDDFT can become especially important for simulations of radiation effects, because these typically do involve electronic excitations e.g. in the form of the electronic stopping power.

2.2 Examples

2.2.1 Proton stopping in nanotubes

In graphitic structures, the Fermi velocity $v_F = 8 \times 10^5$ m/s, which, assuming hydrogen as a projectile, corresponds to ion energy of around 3 keV. Although the role of non-adiabaticity is, to some extent, smeared out due to good conducting properties of nanotubes, several attempts have been made to assess the role of electronic excitations in ion collisions with carbon nanostructures [76–78].

The advantage of the TDDFT approach is that it explicitly takes into account the electronic structure of the target and thus discriminates among

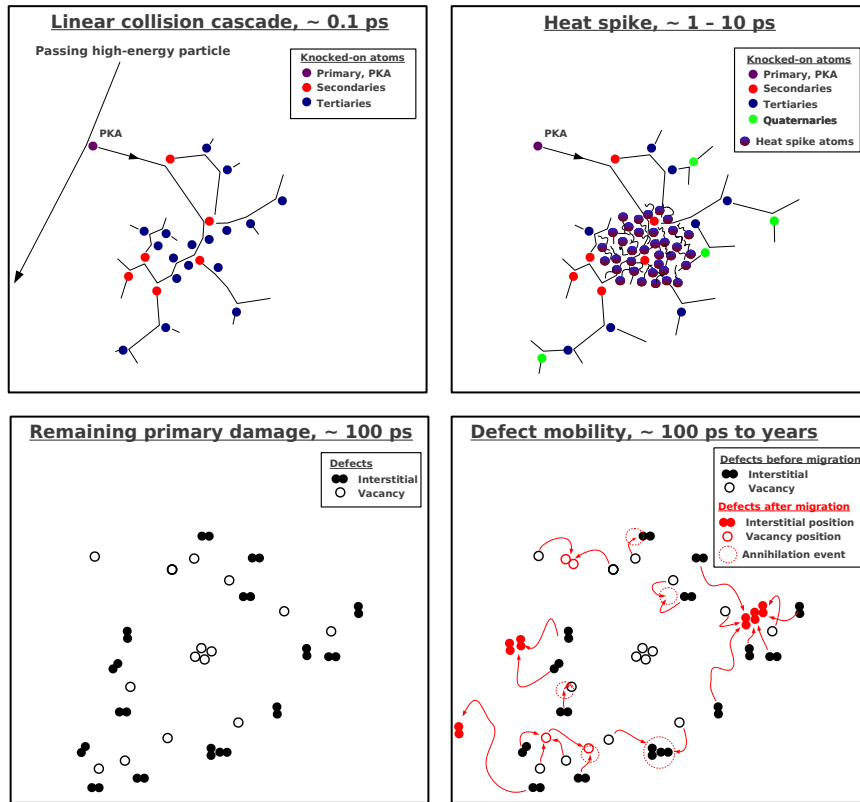


Fig. 2 Schematic illustration of the development of damage in a material induced by an energetic particle. The initial particle can be a gamma quantum, electron, ion, neutron, or some other more exotic particle or particle agglomerate. In ion-induced collision cascades in keV energies, the initial particle often becomes part of the cascade itself. The first atom in the material that receives a recoil energy from the passing particle is called the primary knock-on atom (PKA). Initially the collision cascade may be treated as a set of independent binary collisions (top left). If the initial PKA energy is at least keV's and the material is dense, a very dense region of many-body collisions, i.e. a heat spike (top right) may form. In any case the high-energy collisional phase is over in a few ps to a few tens of picoseconds. After this athermal primary damage phase, defect migration (bottom right) may occur up to macroscopic timescales. In the bottom right image, the red lines illustrate atom migration paths, and the red defect symbols the state of the damage after some given time for defect migration. In reality, the defect motion is a random walk zigzagging in the lattice on much more complex paths than the schematic ones shown in these images. All defects are in principle mobile, but some mobility energies may be so high that the defect system becomes immobile and stops evolving for all practical purposes at a fixed temperature. In this particular illustration, the end result (bottom right) at the given time is one immobile tetravacancy (white open circles in center), one immobile tri-interstitial (filled red double-circles), one immobile di-interstitial, one immobile divacancy (red open circles) and one mobile single interstitial.

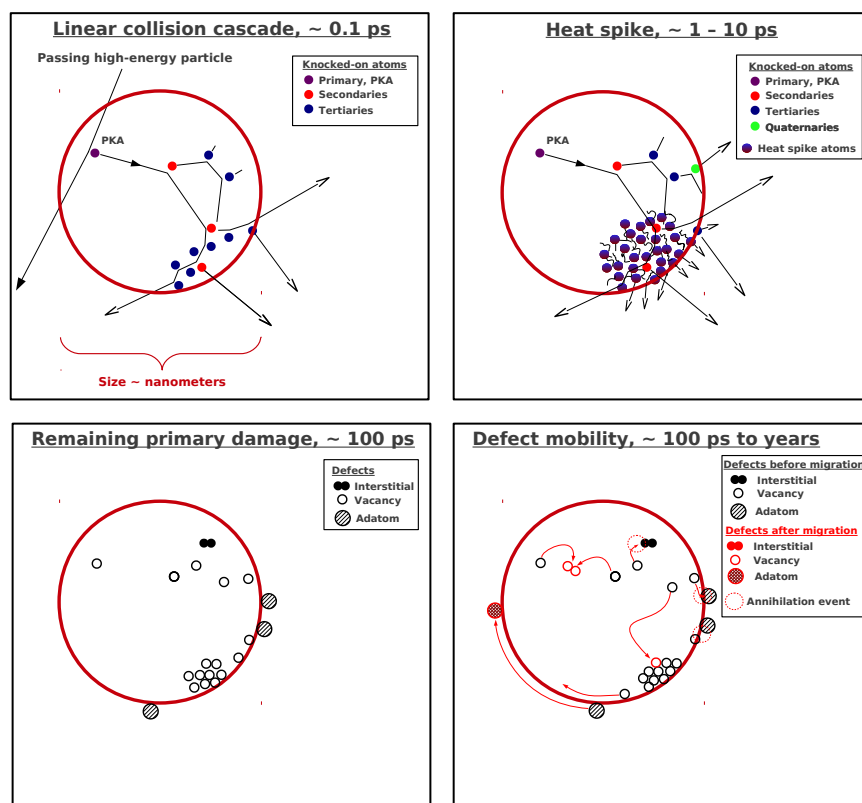


Fig. 3 As Fig. 2 but for a nanostructure, the extent of which is illustrated with the dark red circle. The cascade is assumed to start with the same trajectory as in the bulk case. The figure illustrates how the cascade development can change in a nanostructure due to the presence of the surface. In the linear collision cascade phase (top left), the primary knock-on atom and several other recoils sputter at the surface (large straight arrows). Also the heat spike (top right) can be confined by the surface, leading to enhanced sputtering (smaller straight arrows). Due to sputtering and adatom formation (bottom left) the vacancy production is enhanced and interstitial production reduced compared to the bulk case. The long-term migration is naturally also changed, and damage recombination is reduced as sputtered atoms are lost from the system. In this particular illustration, the end result at the given time is one immobile near-surface vacancy cluster with 10 vacancies, one immobile divacancy, one mobile surface vacancy (white circle with arrow) and one mobile adatom. For nanostructures embedded in a bulk matrix, the behaviour can be expected to be somewhat similar except that the surface is replaced with the interface to the surroundings, sputtering corresponds to ejection of atoms to the matrix, and recoils from the matrix can also end up in the nanostructure (mixing).

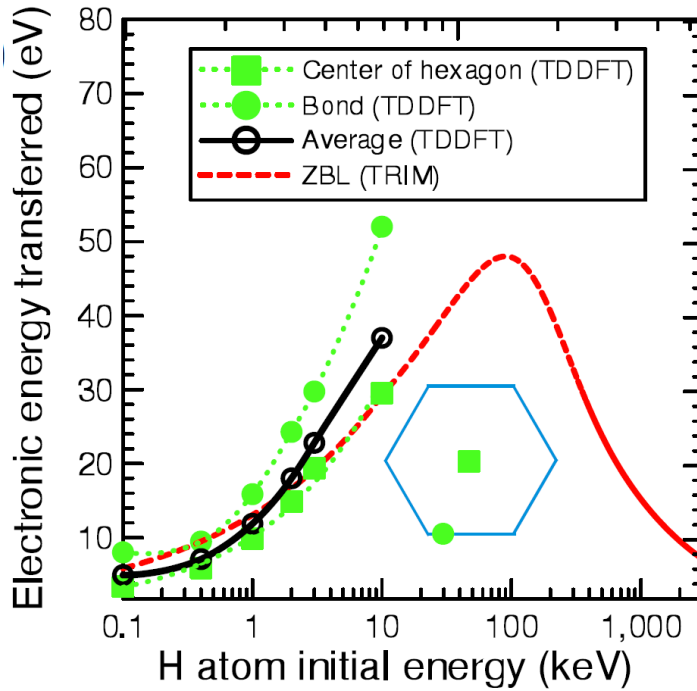


Fig. 4 Stopping in individual trajectories calculated from TDDFT calculations compared to the empirical, tabulated stopping power in the SRIM code for carbon nanotubes. The inset shows the two impact points in one hexagon in the nanotube treated by TDDFT. From Ref. [76].

different carbon allotropes, including diamond and graphite. In addition to radiation simulations, the method has proven useful to describe photo-chemical processes [81] and understand the damping mechanism of electronic excitations [82] in carbon nanotubes.

The results on electronic stopping in carbon nanotubes [76] showed that in individual trajectories there may be large differences in the electronic stopping. However, the average stopping was quite close to the “standard” tabulated stopping power for protons in carbon given by the SRIM code, see Fig. 4.

2.2.2 Electronic stopping in LiF

Electronic stopping in LiF has been studied extensively, primarily because it has a relatively simple electronic structure. This makes it relatively easy to study theoretically, and at the same time it is available in high-quality single crystals for experiments [83–85, 79, 86, 87]. In the most recent theoretical study [79] TDDFT was used to calculate the electronic stopping for protons and antiprotons. The behaviour of the electronic stopping power versus projectile velocity displays an effective threshold velocity of 0.2 atomic units for the pro-

ton, consistent with experimental observations in Ref [85–87]. The projectile energy loss mechanism was reported to be extremely local.

Taken together, these described studies indicate that TDDFT is emerging as a promising tool to examine electronic stopping in materials from first principles. However, most TDDFT studies so far have calculated stopping values for individual trajectories and/or channelling directions. To get an average stopping comparable to SRIM or the experimental stopping powers it is based on, one still needs to calculate the average over many different trajectories, which remains a computational challenge. Nevertheless, as computer capacity and TDDFT algorithms improve, we find it likely that these calculations will shed much additional light also on heavy ion stopping.

3 Density functional theory and tight binding

3.1 Method

The DFT approach [88] is based on two theorems by Hohenberg, Kohn and Sham, which state that (1) the ground state energy of a non-degenerate electronic state is a unique functional (so called density functional) of its density and (2) the energy can be obtained by variation of the universal density functional with respect to the charge density. This implies that calculation of the wave-function of the many-electron system is not required in order to find the total energy, but that it is enough to know only the charge density. This dramatically reduces the computational complexity compared to solving the true all-electron Schrödinger equation. However, the exact density functional is not known and many different approximate functionals are used instead. Often these are chosen based on what compares best to experiments, and thus DFT is not necessarily a fully *ab initio* method in the sense of using no empirical input.

DFT-based and other quantum mechanical methods (e.g., Hartree-Fock methods) have a high accuracy but are computationally very expensive; simulations are normally limited to systems composed of a few hundred atoms and picosecond time scales. This makes the use of such methods in practice impossible for tackling most radiation-related problems, e.g., formation of defects under radiation or direct dynamical simulations of defect diffusion. However, in some limited low-energy cases direct simulation of radiation-induced defect production has recently become possible, and one of these will be reviewed in the examples given below.

3.1.1 Tight-binding methods

As all *ab initio* methods are computationally very demanding, a number of computationally cheaper methods have been developed, such as tight-binding (TB) techniques. In the TB method, the energy is calculated by solving the Schrödinger equation for electrons in the field of atom cores, although the exact

many-body Hamiltonian operator is replaced with a parametrised Hamiltonian matrix. The basis set usually is atomic-like so that it has the same symmetry properties as the atomic orbitals.

A non-orthogonal self-consistent-charge (SCC) TB method [89,90] in which the parameters of the Hamiltonian were derived from DFT calculations (a second-order expansion of the Kohn-Sham total energy in DFT with respect to charge density fluctuations) has been developed that has no empirical parameter. Despite the approximations made, this method retains the quantum-mechanical nature of bonding in materials, ensuring that the angular nature of the bonding is correctly described in far-from-equilibrium structures. Due to parameter fitting to the density functional results, this method, unlike other tight-binding schemes (where the parameters are chosen to describe equilibrium structures) describes the interaction of atoms even at relatively small interatomic separations, i.e., upon energetic collisions.

The SCC TB methodology has been successfully applied to simulations of radiation effects in covalently bonded systems such as silicon, graphite, or hexagonal boron-nitride. It has been widely used for simulations of impacts of energetic electrons onto C [91–93], BN [94], and SiC [95] nanosystems. Another widely used parametrisation for carbon by Xu *et al.* [96] has been successfully applied to simulations of radiation effects in carbon nanomaterials [97–99].

3.2 Examples

3.2.1 Defect energy calculations

The end result of radiation on materials is almost always defect production. DFT is in most solid state cases the most fundamental approach that can be used for practical calculations of defect properties. The basic DFT approach of energy minimization of the electronic and atomic systems is in principle very well suited for calculating the ground state properties of defects, such as the atomic structure, bond lengths, defect formation and relaxation energy and the electronic structure (including energy levels introduced in the band gap in semiconductors and insulators). However, the results are not always fully accurate. Basic DFT approaches tend to underestimate the width of the band gap [100,101] in semiconductors and insulators, leading obviously to problems in the reliability of the defect levels. Recently approaches such as the “LDA+U” [102] and hybrid functionals [103,104,100] have allowed for significant improvement in the treatment of band gaps.

The literature on DFT calculations of point defect properties in materials is vast, and it is well beyond the scope of this article to attempt a comprehensive review of them. To give a flavour of the wide range of materials for which such calculations have been done, we cite here only a few calculations in different classes of materials as examples. Defects properties have been studied with DFT in elemental metals [105–107], metal alloys [108–110], elemental semiconductors [111–113], compound semiconductors [114,115], insulators [116–118].

However, more recently they are widely used to study the properties of nanostructures such as carbon nanotubes [119–122], graphene [123–125], and other two-dimensional materials [126–128].

3.2.2 DFT molecular dynamics of damage production

Although DFT has proven to be a good tool to study the equilibrium ground state properties of defects, the numerical values of these properties alone cannot answer the question of how much defects are produced during the highly non-equilibrium kinetics induced by radiation (Fig. 2). Even at the very lowest energies, the damage is produced in a complex many-body collision process. This is clear from the simple observation that the experimental threshold energies for damage production (also known as displacement energy) is much higher than the thermodynamic formation energy for a Frenkel pair. For instance, for Cu the reported Frenkel pair formation energies are of the order of 4.1 – 5.5 eV [64] whereas the minimum threshold displacement energy is 19 eV [129].

It has recently become possible to use the DFT approach to study dynamic processes that take place during irradiation. By combining DFT and the MD algorithms to simulate atom motion (see section 5) [130,131] it has, in particular, become possible to simulate the threshold displacement energy in materials. Initial simulations showed that at least in low-index directions, the “sudden approximation” (i.e. calculating the energy barrier for a recoil with all other atoms in static positions) may give a reasonable good approximation of the threshold energy [132].

More recently, DFT simulations of thresholds averaging over all lattice directions showed that in Si the average threshold energy is much higher than the minimum of 12 eV. However, it was also detected that one can define two different average thresholds: one considering formation of bond defects (essentially two Si atoms rotating about 90 degrees and then reforming the covalent bonds to form again a fully tetrahedrally bonded system [133–135]) [133,134] at 24 eV, another one considering formation of only Frenkel pairs at 35 eV [112]. Which one should be used depends on the ion flux and sample temperature, as the bond defect is likely less stable than a Frenkel pair [133,134].

Threshold displacement calculations in graphene have shown that by considering also atomic vibrations, one can obtain excellent agreement with experiments on the cross section for damage production [124]. Moreover, the same series of work showed that even below the threshold for atom sputtering from single graphene layers, irradiation can lead to bond rotation (“Stone-Wales”) defects in graphene [136] as well as boron nitride monolayers [137]. This observation has an interesting analogy with the observation of the bond defects having a lower threshold in Si (see above), as these also can be understood to form by bond rotation.

DFT simulations of thresholds in GaN have shown that on both the Ga and N sublattices, the average threshold is roughly two times larger than

the minimum threshold [138], similar to the case of Si. These simulations also showed that there is a major difference with classical potential results of thresholds in GaN [139, 140].

4 Binary collision approximation

4.1 Method

The binary collision approximation is the oldest computer simulation approach for calculating the passage of ions in solids [141, 142] and actually lead to the discovery of channelling in solids [141, 143]. In this approach, the passage of an ion is calculated as a sequence of independent binary collisions by solving the classical scattering integral for purely repulsive interatomic potentials [142, 3]. The BCA code TRIM/SRIM [39, 144, 145] is widely used in the field due to its convenient graphical user interface and extensive database of electronic stopping powers. It uses a random (“Monte Carlo”) algorithms to select the impact parameter of the next colliding atom as well as its type. The solution of the integrals of motion (the key step in BCA simulations) results in precise scattering angles for both the projectile and the target atom. Hence it can describe fairly accurately amorphous materials. Some BCA codes can also describe crystals, such as MARLOWE [142, 146] and “Crystal-TRIM” [147], where the crystallinity is usually given by the ordered lattice sites with the atoms either frozen or oscillating with the Debye frequency.

The BCA method has several limitations. It is not able to distinguish when a cascade goes over from the linear cascade to the heat spike regime, but keeps treating the collisions as independent binary collisions regardless of the collision density. Although it can be used to estimate damage production (basically by counting recoils that exceed the threshold displacement energy) [148], it cannot tell anything about the atomic structure of these defects. The description of sputtering or other surface effects (important in nanosystems) is problematic as the inherent algorithm does not have a unique way of describing the atom binding at surfaces [149, 150]. Nevertheless, the code often gives reasonable deposited energy and range distributions and primary recoil spectra for a wide range of materials [151–157], including nanotubes and nanoclusters [158–160]. Furthermore, as it is orders of magnitude more efficient than molecular dynamics range calculations [161–164] or full MD cascade simulations (see Section 5.2.1), it will remain significant for calculating high-energy ion behaviour for the foreseeable future. In the multiscale scheme this method can be used combined with MD simulations [165–167]. to achieve treating multiple scales in dimensions during high energy ion irradiation. For instance, in the approach taken in Ref. [165] the high-energy (larger than several 10 eV) ion and recoils were treated with BCA, but the regions where the recoils are thermalized treated by several separate MD simulations. This kind of an approaches can allow treating damage morphology development along the entire ion trajectory even for very high-energy (MeV) ions.

4.2 Examples

4.2.1 Calibrating BCA Damage production models

Description of defect production in dense metals such as Fe and Cu is particularly problematic for BCA simulations, as in-cascade defect recombination in heat spikes plays a big role on the damage production [44]. This typically reduces the damage to a factor of about 0.3 (known as the damage efficiency [44]) of that what would be predicted in a simple BCA model [168]. However, it is possible to include a separate model of defect recombination in BCA simulations by analyzing for closeby pairs of vacancies and interstitials and making these recombine [169]. Heinisch combined MARLOWE BCA simulations with a Monte Carlo recombination code in a way that can reproduce the damage efficiency of about 0.3 in Cu [169]. However, it is important to realise that such an approach still cannot reproduce the formation of ordered defect structures such as stacking fault tetrahedra [170].

More recently, Pelaz *et al* have systematically used MD cascade simulation to calibrate BCA models to provide an efficient yet realistic prediction of defect generation and the nanometer-scale spatial distributions in Si [171–173], which is described further in section 6.2.3.

5 Molecular Dynamics

5.1 Method

Molecular dynamics (MD) simulations involve numerical solution of the Newton equations of motion to determine the time evolution of a system of interacting objects [130, 131]. The name is somewhat misleading as the method does not necessarily involve molecules at all, and in fact basically the same approach can be used even to simulate the formation of galaxies [174]. It is a very widely used method to study all kinds of atomic-level physics, chemistry and biological issues, and (contrary to BCA) by no means specific to radiation effects.

The simplest variety of MD, direct solution of the equations of motion, is ideally suited to study ion-induced radiation effects as this scheme correctly accounts for the non-equilibrium ballistic motion of high energy ions as well as the subsequent thermalization of the ion [44]. Moreover, with current computers it is possible to simulate the entire extent of collision cascade evolution both in space (up to length scales of hundreds of nanometers in three dimensions) and time (up to nanoseconds) [175].

Efficient realistic simulation of radiation effects, however, requires the basic MD methods [130] to be amended with a few solutions specific to radiation effects. These may account for electronic stopping as a frictional force, [162] realistic high energy repulsive interactions [39] (see above) and making the time step adaptive to the maximum kinetic energy and force in the system in

the ballistic phase of the cascade,[162] while reducing it to a normal constant equilibrium time step after the cascade.

To dissipate the heat emanating from the cascade away from the simulation cell, temperature scaling (velocity damping) at the boundaries is often carried out, although sometimes this step is left out and the temperature is simply allowed to spread out in the simulation cell. If the cell is large enough that the associated temperature rise is not significant, this can be considered acceptable. Multiple-time step schemes [176] may be useful for speeding up the initial stages of the simulation when atoms have highly disparate velocities.

MD simulations require the forces as the starting point for solving the equations of motion. The forces can be obtained from DFT or with classical interatomic potentials. As DFT MD simulations are still limited to a few hundreds of atoms, classical (empirical, analytical) potentials remain the method of choice for high-energy radiation effect simulations, as these typically involve at least tens of thousands of atoms. These potentials involve a set of analytical equations or spline functions [177] with parameters fitted to empirical and/or DFT data. Potentials exist for a wide range of systems. However, when simulating radiation effects it is crucial to select potentials that allow for bond breaking and reformation, ruling out the use of most molecular mechanics force fields [178]. For carbon-based systems, the Brenner potential [179] and its extensions [180,181] as well as the ReaxFF formalism [182] allow for bond breaking. For metals the Finnis-Sinclair and embedded-atom method potentials and their functional equivalents are widely used, [183–187] while for covalently bonded materials Tersoff-like bond order potentials [188,179,189] have proven to be quite successful. For compounds of different types of materials far fewer potentials are available, but since the Tersoff and Finnis-Sinclair-like potentials are fundamentally similar [179,190], a Tersoff-like formalism has proven to be useful in development of potentials for carbides, oxides and nitrides.[190–194]

Although these potentials have been fitted to reproduce a large number of reference systems, the drawback of the empirical approach is its low transferability (the ability to describe systems different from those used for fitting the parameters, for example, correctly describe defect behaviour). Nevertheless, the methods have been demonstrated to give valuable results for a wide range of materials science studies [195–202].

5.2 Examples

5.2.1 Simulation of collision cascades in the bulk and nanostructures

As noted above, the MD method is well suited for studying collision cascades, and indeed it has been widely used for this purpose [204–207,45,68,208,209,73,210–215,57,216,217]. Snapshots of a particular case of a 2 keV cascade in silicon are shown in Fig. 5, and several animations of cascades are read-

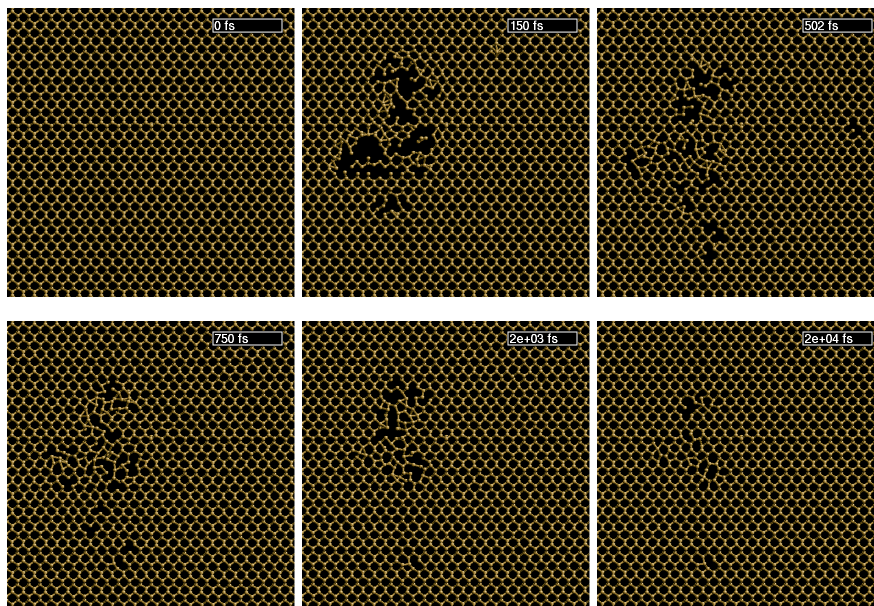


Fig. 5 Snapshots of a molecular dynamics simulation of a collision cascade in bulk Si, shown to give a point of reference to the nanostructure cases shown later. The frames show a 2 atom layers thick slice of the simulation cell. Note how some of the damage created in the cell regenerates during the course of the cascade. The simulation was carried out following the principles in Ref. [203].

ily available for easy viewing in youtube.com by searching for “displacement cascade”.

The MD simulations of cascades have given several key insights on how the primary damage state in materials is produced. Already some of the very first MD simulations ever done lead to the concept of “replacement collision sequences” [204] and showed that the threshold displacement energy is highly direction-dependent [205]. When computers became efficient enough to handle tens of thousands of atoms MD simulations showed how a cascade core becomes underdense [45] as originally postulated by Brinkman [218]. Simulations of near-surface cascades in the heat spike regime showed how experimentally observed craters [66] can form by explosive and liquid flow mechanisms [68, 54]. Similarly, cascade simulations in Si showed how single ions can produce amorphous regions in semiconductors [208], something observed earlier experimentally [49]. Simulations in compounds have shown that there can be large asymmetries in the number of primary defects produced [219, 220].

With advances in computer capacity, the possibility to simulate increasingly large systems of atoms by means of MD methods, has opened the unique opportunity of “one-to-one” simulation of nanostructures at exactly the same size as that studied experimentally. Simulations of sputtering of nanoparticles have shown that for a fixed ion energy, in very small nanoparticles the sputtering yield was decreased compared to the bulk sputtering yield due to ion

transmission. With increasing energy the yield increased above the bulk yield due to the large surface-to-volume ration [221]. Similarly, studies of damage production and sputtering in nanowires (cf. Fig. 6) have shown that there is an ion energy at which the damage production has a maximum, above which the damage decreases due to ion transmission [222,223], see Fig. 7. Indeed, recent experiments have confirmed that there can be a major (more than a factor of 10) enhancement of the sputtering yield of nanowires compared to bulk [224].

Collision cascades in carbon nanotubes has been studied extensively by MD simulations (for reviews see e.g. [226,6]). The results have, among many others, shown that in single-wall nanotubes no real interstitials exists, but adatoms behave much like them [227,228] and that vacancies can have different reconstructed shapes [227,229,230]. Simulations of prolonged radiation have elucidated how nanotubes can be welded together by irradiation [231], stiffened by irradiation [232], and used as masks [233] against irradiation of a substrate. They have, together with experiments, also shown that the shrinkage of multiwall tubes by irradiation can be used to make them act as a pressure vessel on metals encapsulated inside them [234,235].

5.2.2 Multiscale modelling of swift heavy ion tracks

When the energy of ions becomes very high ($\gg 10$ keV/amu), the electronic stopping starts to dominate over the nuclear stopping. If the ion is heavy and the target material is sufficiently dense that the electronic stopping power exceeds about 2 keV/nm, purely electronic processes may start producing damage [40,41]. This damage typically takes the form of long straight cylindrical regions which appear as nanometer-wide tracks in a cross-sectional electron microscope image.

The process by which swift heavy ions produce damage is very poorly understood. Three fundamentally different mechanisms for the damage creation have been proposed. These are, in very brief summary: (i) heating of the track core due to electron-phonon coupling from the electronic excitations [236,237,41], (ii) a Coulomb explosion caused by many electrons being rapidly excited out of the core due to the passing ion [238], and (iii) “cold melting”, i.e. electrons being excited into antibonding states causing bond breaking [239,240]. These are dramatically different in that the former method explains everything by rapid heating of the track core into temperatures of the order of 100 000 K, while the latter states that the material can be damaged even if the temperature never exceeds the melting point of about 2 000 K.

Although it is very challenging to determine which model is correct (and it seems likely the true picture is some combination of them [241]), the models can be implemented as concurrent multiscale schemes within a molecular dynamics code. The electron-phonon coupling models (i) can be implemented as a two-temperature scheme where a continuum diffusion equation is used to solve the electronic heat conduction equation, and the MD equations take inherently care of the lattice heat conduction. The coupling between the two

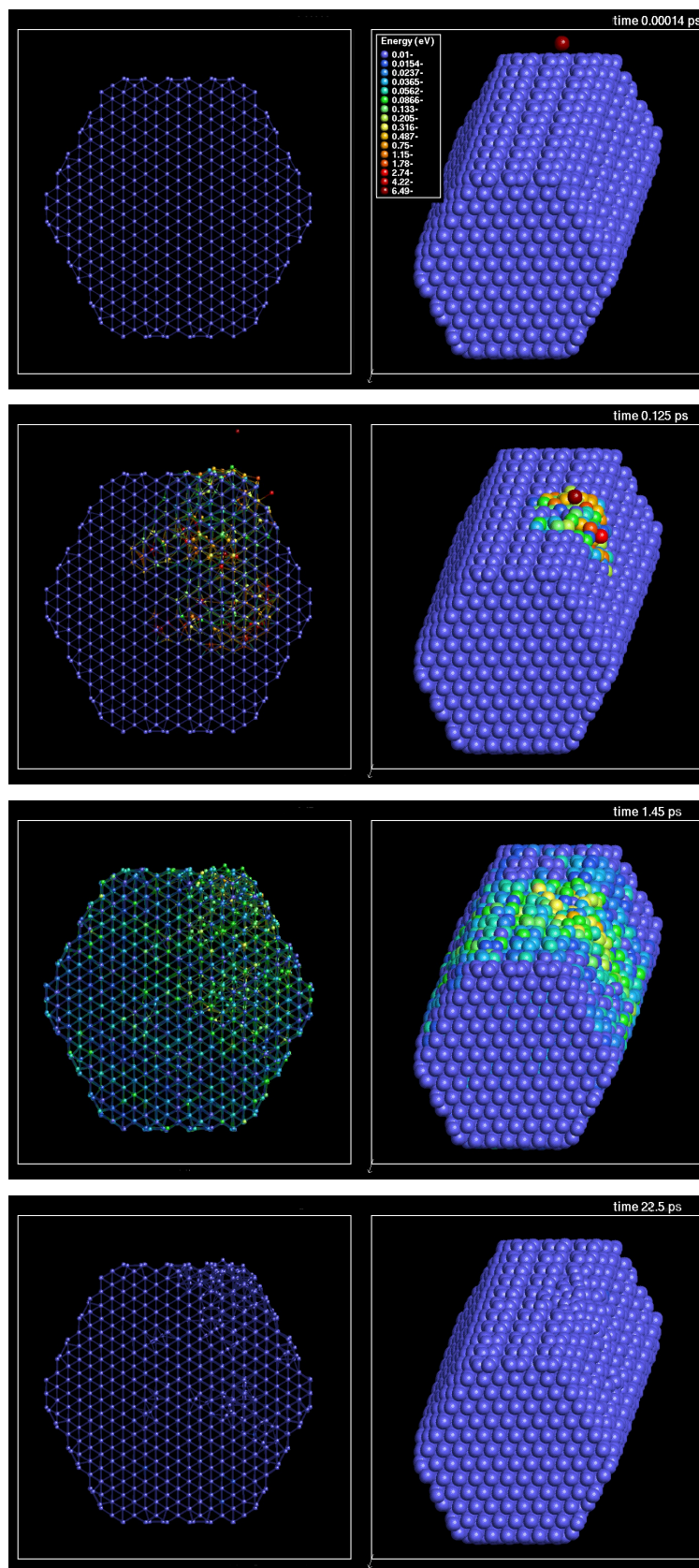


Fig. 6 Snapshots of a molecular dynamics simulation of a collision cascade in a Si nanowire induced by a 1 keV Ar ion. The left sides show a through-view of the entire nanowire and the right sides exactly the same nanowires in a 3D view from above. The atoms are coloured according to their kinetic energy. Data from simulation made for Ref. [222].

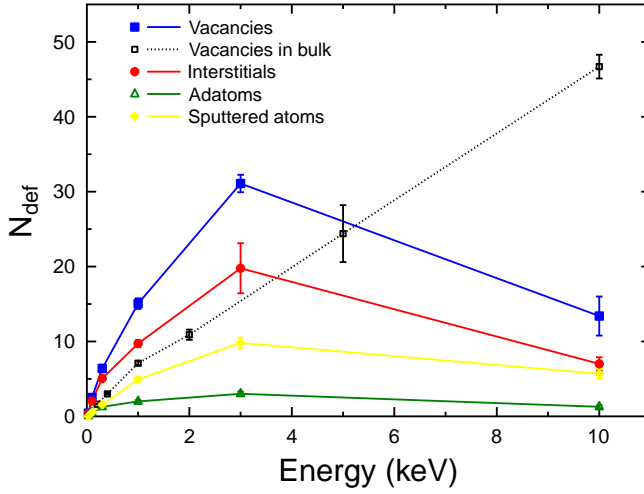


Fig. 7 Defect production in a 3 nm diameter GaN nanowire as a function of energy. Note that in the reference case of damage by Ga ions in bulk GaN [225], the defect production increases linearly with ion energy in this energy range. The nanowire data is from [223].

systems is taken into account as a stochastic force affecting the atom motions with a magnitude related to the electron-phonon coupling (EPC) [242–244]. A Coulomb explosion model can be implemented by giving atoms enhanced charges and letting them interact via a Coulomb potential [241, 245, 246]. Cold melting, which involves the breaking of chemical bonds via electronic excitations, is challenging to implement in classical MD. However, it can be somewhat mimicked by introducing time-dependent changes in the interatomic potential [247–249].

As part of a recent study on the formation of voids induced by swift heavy ion irradiation, a 3-level concurrent multiscale modelling scheme was used to model swift heavy ion effects on amorphous Ge [249]. At first, an asymptotical trajectory Monte Carlo (ATMC) method [250] was used to simulate the generation and dynamics of the δ -electrons formed by the passing swift heavy ion. The ATMC simulations considered the high-energy (> 5 eV) electrons, and were run in parallel with a two-temperature model (TTM) simulation of the diffusive transport of the lower-energy electrons. When the energy of the explicitly treated MC electrons falls below the 5 eV cutoff, this energy is removed from the MC and added to the TTM model. The TTM model was also used to describe the EPC, i.e. the coupling of the electron and phonon subsystems. Finally, the energy transferred to the “phonon” subsystem from the ATMC-TTM simulations was given as kinetic energy to the atoms in an MD simulation [249].

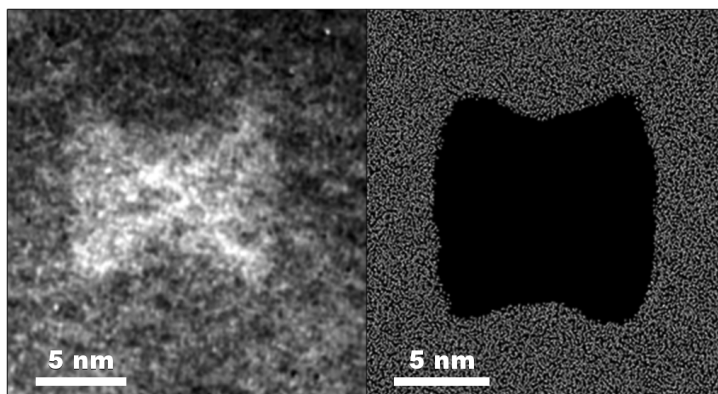


Fig. 8 Left: experimental TEM image of a bowtie-shaped void formed by swift heavy ion irradiation of amorphous Ge. Right: simulated image of a void formed during the same radiation conditions. The data used for the images is the same as in Ref. [249].

The MD simulations, when using a combination of potentials that described well both the formation of a high-density liquid phase of Ge [251] and the subsequent transition of this phase back to the solidified amorphous phase [252], reproduced excellently the formation of the experimentally observed “bow-tie” shaped void [249], see Fig. 8. The simulations showed that formation of this special void shape can be understood to be due to the balance between the formation of a high-density liquid and the different re-solidification rates of the sides and central region of the ion track [249].

6 Kinetic Monte Carlo

6.1 Method

Comparison of MD data with experiments is often complicated by the limited time scale of the MD simulations. The basic MD time step is of the order of 1 fs, and can not be increased in a general non-equilibrium situation (although for systems involving well-defined transitions from one state to another, several speedup schemes exist [253–255]). Hence the requirement for computational time increases linearly with the physical time one wants to simulate, limiting most MD simulations to nanosecond time scales. As a direct consequence of this, most diffusion processes and long-term relaxation of molecular structures are not accessible by MD.

Kinetic Monte Carlo (KMC) methods can sometimes solve this problem [256–259]. The method takes as input the rates of relevant processes in a system, which typically are the defect migration rates and incoming ion flux, and simulates the time evolution of the objects. The algorithm selects the processes proportionally to their rates, so no effort is wasted in time steps with no events occurring.

The time in KMC advances stochastically, but on average as $\Delta t = 1/R$ where R is the sum of all rates r_i in the system. Hence if fast-moving objects vanish from the simulation due to e.g. recombination, the high values of r_i vanish from the sum $R = \sum r_i$. This makes R decrease and hence the time advancement Δt increase. Thus a KMC simulation may speed up in the evolution of real time as a system develops, making for a major difference with MD simulations.

In atomic kinetic Monte Carlo (AKMC) simulations all atom coordinates are included but only one or a few defects (typically vacancies) at a time are moving [260]. In other modifications of the method, only the mobile defects are followed, and the lattice atoms are not explicitly described at all (such methods are known as object, reaction, event, or first-passage kinetic Monte Carlo, i.e. OKMC, RKMC, EKMC [261] or FPKMC [262], respectively). Since only the objects of interest are simulated, this allows for simulation of macroscopic time (up to several hours) and length scales.

6.2 Examples

6.2.1 Defect mobility in carbon nanotubes

An AKMC approach which is used for simulations of the response of a nanosystem to ion or electron bombardment should allow for sputtering and other radiation-induced effects. Such a method was developed in Ref. [259]. It enabled one to simulate the behaviour of irradiated nanotubes on macroscopic time scales, Fig. 9. Within the model, the paths and energy barriers for the diffusion of radiation-induced defects are obtained from DFT-based calculations [263,264].

Simulations run with this model indicated that at temperatures higher than 300 °C, the annihilation of defects is efficient enough for almost perfect in situ self-healing of nanotubes, in perfect agreement with experiments [264]. They also allowed to simulate what kind of electron irradiation fluences are needed to cut a single-walled nanotube, and showed that these values also agree well with experimental values [264].

6.2.2 Deposition simulations by on-the-fly KMC

The KMC method has the major drawback that it requires as input the rates of all processes occurring. In most cases these are obtained prior to the start of the KMC scheme, but in this case configurations that have different transition barriers than the input one cannot be included in the simulations. In so called “on-the-fly” approaches, some other simulation tool, that can determine the transition barriers as the atomic configurations change, is run concurrently with an AKMC one.

In a particularly promising implementation, the search for transition barriers is done in a client-server parallel approach, such that a large number

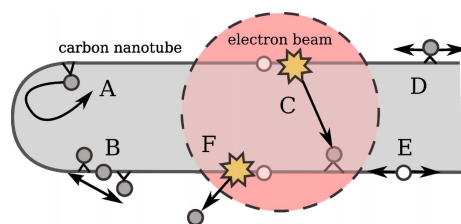


Fig. 9 Schematic description of the most important processes included in a KMC model [259] developed to simulate the response of carbon nanotubes to electron irradiation. The model includes the following 'elementary' events: (A) A diffusing endohedral adatom is reflected back from a cap. (B) Endohedral-exohedral transformation of an adatom through the exchange mechanism. (C) Electron impact creating a defect pair (white sphere - a vacancy, gray sphere - an adatom) by displacing a carbon atom. (D and E) Adatom and vacancy migration, respectively. (F) Creation of a vacancy by sputtering the displaced atom.

of processors search for the transition barriers simultaneously [255]. The saddle points are searched for with a relaxation-and-translation method (RAT) followed by a nudged-elastic band (NEB) calculations [265] to obtain the transition barrier more accurately. The interatomic interactions are obtained from classical interatomic potentials. Once a sufficient number of transition barrier candidates have been found, the corresponding rates are calculated with an Arrhenius equation. These rates are then used as the inputs for the next KMC step. The determination of the transition barriers is the slowest part of the simulation, but these searches can be trivially parallelized. The parallel implementation can make for a major speedup of the simulations [255].

Using this approach, simulation of the growth mechanisms of Al and Ag nanometer-thin films could be carried out at realistic experimental fluxes. This is a major achievement compared to conventional MD which typically overestimates the flux by ~ 5 -10 orders of magnitude. The results illustrated e.g. the difference between thermal evaporation and magnetron sputtering deposition, see Fig. 10 [255]. The simulations also showed that under some conditions, ion-beam assisted growth can lead to the formation of nanosized voids in the material [255].

6.2.3 Modelling of Si processing

Kinetic Monte Carlo methods have found a very good application in simulation of Si processing stages, since ion implantation is routinely used to introduce the dopants into Si that enable its use in the electronics industry [7]. As the size of the active parts of the transistors used in Si chips have shrunk to the nanometer scale [8], the number of doping atoms becomes so small that atom-level fluctuations in the number of doping atoms starts to become significant for the device operation. Hence atom-level simulation tools are significant to understand these effects.

The Si processing sequence typically involves an ion implantation that amorphizes the material, followed by a high-temperature annealing that has

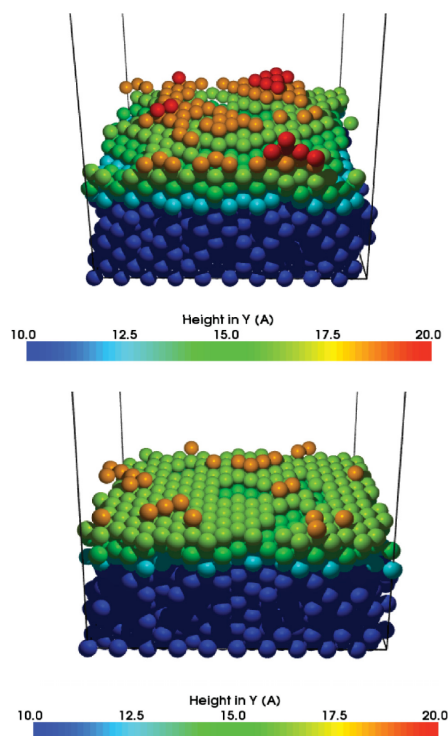


Fig. 10 Difference between growth of Al (100) by evaporation (top) and sputtering (bottom) simulated with an on-the-fly KMC technique up to a time scale of 0.23 s. The images are from Ref. [255]. Reprinted with permission from author. Copyright (2012) by The American Physical Society.

two important functions: recrystallization of the Si as well as placing the dopant atoms on substitutional sites, where they have the desired electrical functionality [266,7]. However, the details of this process are fiendishly complex, as both the amorphization [48,267] and recrystallization [268,7,269,270,62,271,63] involve several intermediate stages.

In a long-running systematic effort, Pelaz *et al.* have developed a multiscale modelling framework for describing the entire Si amorphization, recrystallization and dopant activation process [272,271,273–276,171–173,277].

In this approach, the implantation cascades are simulated with the BCA code MARLOWE [142], which has been parametrised from MD simulations to give a reasonable estimate of the intrinsic defect concentrations [173]. The coordinates of the Si self-interstitials and vacancies obtained from MARLOWE are transferred to an off-lattice KMC code [278,279]. In this KMC code, the mobile diffusing objects are either point or extended defects in Si. The clusters of point defects are formed when the mobile point defects jump inside the capture radius of other point defects or pre-existing clusters [275]. The disso-

lution of defects occurs by emission of a point defect at a rate determined by the binding energy of this defect. The energies used in the KMC simulations are obtained from DFT calculations or estimated by fitting experimental data [268,270]. The surface is considered as a sink for point defects, in agreement with experimental evidence [280]. After each cascade introduces new defects, annealing is carried out during a time defined by the dose rate of the implant. This takes into account the annealing during the implant and thus, the influence of implant parameters on damage accumulation [274,275].

This model has been successfully used to examine a wide range of issues of Si implantation, such as the recrystallization mechanisms [275] and the behaviour of 311 defects during such recrystallization [274], see also Fig. 11. The amorphization of Si is modelled in an ingenious way. At first sight, it might seem that an object KMC model which has point defects as the basic object cannot describe amorphization. However, the bond defect [133–135] (cf. section 3.2.2) which breaks the lattice symmetry but retains fourfold coordination of all atoms offers a way around this dilemma. In their modelling, Pelaz et al consider buildup of these defects to form amorphous Si [271,275,171], which is consistent with the picture of amorphous Si being a network of tetrahedrally coordinated Si atoms with no long-range order [281,282]. This approach gives good agreement with experimental data on the annealing of Si [171] and provides a possible explanation to experiments which show that amorphous pockets of the same size can have very different annealing behaviour [171,283].

The OKMC model has been also used to describe the behaviour of boron dopants in Si [276,277], including the formation of nanosized boron-selfinterstitial clusters [277]. The results show, for instance, that the presence of such clusters can explain why boron dissolution in Si has been experimentally observed to exhibit two different rates for high B concentrations, see Fig. 12.

7 Concluding remarks

7.1 Summary of simulation methods

The fantastic experimental capabilities of modern nanoscience are actually a boon for multiscale modelling: they can provide experimental test systems that allow for developing and testing the multiscale treatment of the time domain, without the need for multiple scales in space.

The time-wise range of applicability of the different simulation methods discussed in this article can be summarised as follows. The binary collision methods, when they involve both primary and secondary recoil atoms, are well suited for obtaining the spatial extent of the ballistic collisions on sub-picosecond timescales, but cannot tell anything about the thermodynamic aspects of a cascade or detailed nature of defects. In nanosystems, the BCA methods have the further problem that the treatment of a surface or interface (always nearby in nanosystems) is not well defined in the basic algorithm. Molecular dynamics simulations can, in addition to the ballistic phase of the

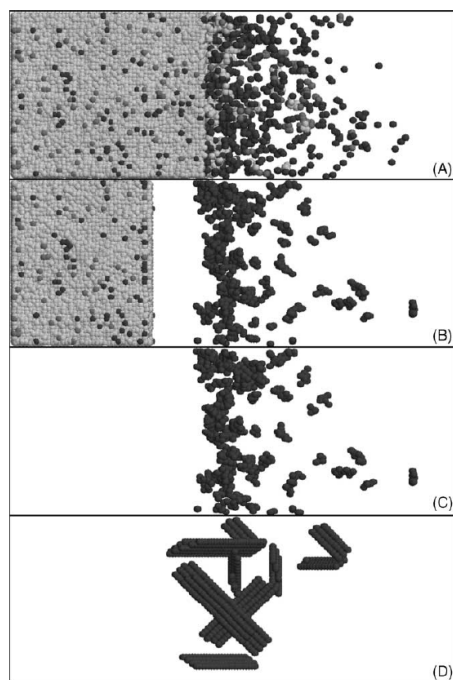


Fig. 11 Illustration of object KMC description of the amorphization and subsequent recrystallization of Si by 5 keV Si self-implantation. Light points represent IV pairs and dark points correspond to Si interstitials and vacancies. (a) Damage after implantation at room temperature. (b) Damage after annealing at 550 C. (c) Defects remaining after regrowth of the amorphous layer. (d) 311 defects resulting after further annealing at 800 C. The image is from Ref. [275]. Reprinted from Ref. [Atomistic modeling of defect evolution in Si for amorphizing and subamorphizing implants, Pedro Lopez, Lourdes Pelaz, Luis A. Marques, Ivan Santos, Maria Aboy, and Juan Barbolla, *Mater. Sci. Engr. B*, 114-115:82–87, 2004] with permission from Elsevier.

cascade, describe the formation of heat spikes, their thermalization, formation of a sound/shock wave and how it spreads beyond the region of ballistic collisions. MD simulations can also predict the nature of defects produced and handle surface effects. However, there are major uncertainties in how reliable classical potentials are with respect to defect and surface types and properties. Quantum mechanical methods (DFT and TB) can provide a much more reliable picture of defect properties, but are quite limited in the number of atoms and time scale they can feasibly handle. The different KMC approaches are well suited to describe atom migration on both space and time scales exceeding those in MD by orders of magnitude, but great effort is often needed to parametrise the KMC reliably. Furthermore, in nanosystems it is quite likely that the nearby surface exerts significant image interactions on defects via the strain field, which complicates KMC implementation.

Electronic and optical excitations can in principle be fully described by TDDFT, but this approach is extremely time-consuming, and treatment of

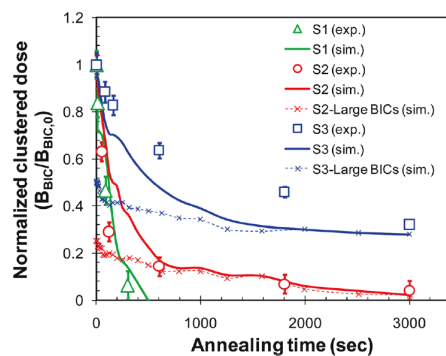


Fig. 12 Results from an OKMC model of the dissolution of boron in Si compared to experiments. S1-S3 stands for increasing boron concentration. The good agreement with experiments for the larger concentrations (S2 and S3) is only obtained when boron-selfinterstitial clusters with more than four B atoms were included in the model, showing that such clusters can explain the slow dissolution of B for high implant concentrations. Reprinted with permission from Ref. [277]. Copyright 2011, AIP Publishing LLC.

all possible excitations, transport and recombination processes in the full collisional phase of a cascade in a dense material will remain beyond reach far into the future. On the other hand, the very small size of thin nanosystems may make it already now possible to treat all atoms near a high-energy ion with TDDFT, and thus get deeper insight into atom stopping processes in experimentally relevant systems.

7.2 Outlook

Although sequential multiscale modelling has been used for a long-time, concurrent multiscale models are still relatively rare. However, they are emerging as a promising way for modelling of radiation effects on both bulk and nanosized structures of unprecedented complexity. Already now several different levels of physics have been implemented in a concurrent model for a well defined system. For instance, for atom emission from sharp straight tips at charged surfaces a concurrent model combining four different levels of physics has been developed [284–286], which could lead to a way to model ion sources. The parallel on-the-fly hybrid MD - KMC approaches are emerging as a promising new solution for being able to simulate ion implantation at experimental fluxes [255]. Modelling of swift heavy ion irradiation effects clearly requires description of both electronic and atomic subsystems, and two-temperature model approaches (possibly later parametrised by TDDFT simulations) are quite promising in this respect [287, 242, 249].

These cases serve naturally just as examples of the rich field of multiscale modelling of radiation effects on the nanoscale, which is rapidly developing and will certainly produce many other examples of innovative ways to examine increasingly complex materials systems and processes.

Acknowledgements We are indebted to several colleagues for numerous useful discussions on the different simulation approaches described in this Article, in particular Doc. Arkady Krasheninnikov and Doc. Antti Kuronen. We thank Ms. Wei Ren for providing the figure on damage production in nanowires.

References

1. ATLAS Collaboration, *Physics Letters B* **710**(1), 49 (2012)
2. CMS Collaboration, *Physics Letters B* **710**(1), 26 (2012)
3. R. Smith (ed.), *Atomic & ion collisions in solids and at surfaces: theory, simulation and applications* (Cambridge University Press, Cambridge, UK, 1997)
4. H.F. Winters, J.W. Coburn, *Surf. Sci. Rep.* **14**, 161 (1992)
5. D. Schulz-Ertner, H. Tsujii, *Journal of Clinical Oncology* **25**(8), 953 (2007)
6. A.V. Krasheninnikov, K. Nordlund, *J. Appl. Phys. (Applied Physics Reviews)* **107**, 071301 (2010)
7. E. Chason, S.T. Picraux, M. Poate, J.O. Borland, M.I. Current, T. Diaz de la Rubia, D.J. Eaglesham, O.W. Holland, M.E. Law, C.W. Magee, J.W. Mayer, J. Melngailis, A.F. Tasch, *J. Appl. Phys.* **81**(10), 6513 (1997)
8. The International Technology Roadmap for Semiconductors, available online at www.itrs.net
9. J.D. Verhoeven, *Scientific American* **284**(1), 62 (2001)
10. X. Huang, W.C. Lee, C. Kuo, D. Hisamoto., L. Chang, J. Kedzierski, E. Anderson, H. Takeuchi, Y.K. Choi, K. Asano, V. Subramanian, T.J. King, J. Bokor., C. Hu, International Electron Devices Meeting Technical Digest p. 67 (1999). DOI 10.1109/IEDM.1999.823848
11. S. Tiwari, F. Rana, K. Chan, L. Shi, H. Hanafi, *Appl. Phys. Lett.* **68**(9), 1377 (1996)
12. L. Pavesi, G. Guillot, *Optical Interconnects: The silicon approach* (Springer, Berlin, 2006)
13. L. Pavesi, L.D. Negro, C. Mazzoleni, G. Franzo, F. Priolo, *Nature* **408**, 440 (2000)
14. L. Khriachtchev, M. Räsänen, S. Novikov, J. Sinkkonen, *Appl. Phys. Lett.* **79**(9), 1249 (2001)
15. E. Cattaruzza, F. Gonella, S. Ali, V. Bello, T. Cesca, *Solid State Phenom.* **151**, 252 (2009)
16. R. Behrisch (ed.), *Sputtering by Particle bombardment I* (Springer, Berlin, 1981)
17. P. Sigmund, *Nucl. Instr. Meth. Phys. Res. B* **27**, 1 (1987)
18. R.E. Johnson, J. Schou, *Matematisk Fysiske Meddelelser Konglige Danske Videnskaberne Selskab* **43**, 403 (1993)
19. T. Schenkel, M.A. Briere, K. Schmidt-Böcking, K. Bethge, D.H. Schneider, *Phys. Rev. Lett.* **78**(12), 2481 (1997)
20. M. Toulemonde, W. Assman, C. Trautmann, F. Gruner, H.D. Mieskes, H. Kucal, Z.G. Wang, *Nucl. Instr. Meth. Phys. Res. B* **212**, 346 (2003)
21. H. Plank, W. Eckstein, *Nucl. Instr. Meth. Phys. Res. B* **124**, 23 (1997)
22. M.P. Seah, T.S. Nunnery, *J. Phys. D: Appl. Phys.* **43**, 253001 (2010)
23. E. de Juan Pardo, M. Balden, B. Ciecwiwa, C. Garcia-Rosales, J. Roth, *Physica Scripta* **T111**, 62 (2004)
24. E. Salonen, K. Nordlund, J. Tarus, T. Ahlgren, J. Keinonen, C.H. Wu, *Phys. Rev. B (Rapid Comm.)* **60**, 14005 (1999)
25. H. Timkó, F. Djurabekova, L. Costelle, K. Nordlund, K. Matyash, R. Schneider, A. Toerkle, G. Arnau-Izquierdo, A. Descoedres, S. Calatroni, M. Taborelli, W. Wuensch, *Phys. Rev. B* **81**, 184109 (2010)
26. J. Küppers, *Surf. Sci. Rep.* **22**, 249 (1995)
27. M.I. Guseva, V.M. Gureev, B.N. Kolbasov, S.N. Korshunov, Y.V. Martynenko, V.B. Petrov, B.I. Khripunov, *Journal of Experimental and Theoretical Physics Letters* **77**, 362 (2003)
28. D.B. Williams, C.B. Carter, *Transmission Electron Microscopy: a textbook for materials science* (Plenum Press, New York, USA, 1996)

29. G. Binnig, H. Rohrer, C. Gerber, E. Weibel, *Phys. Rev. Lett.* **49**, 57 (1982)
30. G. Binnig, C.F. Quate, C. Gerber, *Phys. Rev. Lett.* **56**(9) (1986)
31. K.M. Lang, D.A. Hite, R.W. Simmonds, R. McDermott, D.P. Pappas, J.M. Martinis, *Rev. Sci. Instr.* **75**, 2726 (2004)
32. ITER Physics Basis Editors, ITER Physics Expert Group Chairs and Co-Chairs and ITER Joint Central Team and Physics Integration Unit, *Nuclear Fusion* **39**, 2137 (1999)
33. J. Merikoski, I. Vattulainen, J. Heinonen, T. Ala-Nissilä, *Surface Science* **387**, 167 (1997)
34. F.G. Djurabekova, R.D. R., G. Cerchiara, N. Castin, L. Malerba, *Nucl. Instr. Meth. Phys. Res. B* **255**(1), 8 (2007)
35. F. Banhart, *Rep. Prog. Phys.* **62**, 1181 (1999)
36. S. Dhara, *Critical Reviews in Solid State and Materials Sciences* **32**, 1 (2007)
37. I. Utke, P. Hoffmann, J. Melngailis, *J. Vac. Sci. Tech. B* **26**, 1197 (2008)
38. J. Lindhard, M. Scharff, H.E. Shiøtt, *Mat. Fys. Medd. Dan. Vid. Selsk.* **33**(14), 1 (1963)
39. J.F. Ziegler, J.P. Biersack, U. Littmark, *The Stopping and Range of Ions in Matter* (Pergamon, New York, 1985)
40. D. Kanjijal, *Current Science* **80**(12), 1560 (2001)
41. M. Toulemonde, W. Assmann, C. Dufour, A. Meftah, F. Studer, C. Trautmann, *Mat. Fys. Medd. Kong. Dan. Vid. Selsk.* **52**, 263 (2006)
42. F. Spaepen, D. Turnbull, *Crystallization processes* (Academic Press, New York, 1982), chap. 2, pp. 15–42
43. S. Raman, E.T. Journey, J.W. Warner, A. Kuronen, J. Keinonen, K. Nordlund, D.J. Millener, *Phys. Rev. C* **50**(2), 682 (1994)
44. R.S. Averback, T. Diaz de la Rubia, in *Solid State Physics*, vol. 51, ed. by H. Ehrenfest, F. Spaepen (Academic Press, New York, 1998), pp. 281–402
45. T. Diaz de la Rubia, R.S. Averback, R. Benedek, W.E. King, *Phys. Rev. Lett.* **59**, 1930 (1987). See also erratum: *Phys. Rev. Lett.* **60** (1988) 76
46. A.E. Stuchbery, E. Bezakova, *Phys. Rev. Lett.* **82**(18), 3637 (1999)
47. C. Kittel, *Introduction to Solid State Physics*, 3rd edn. (John Wiley & Sons, New York, 1968)
48. P. Partyka, Y. Zhong, K. Nordlund, R.S. Averback, I.K. Robinson, P. Ehrhart, *Phys. Rev. B* **64**, 235207 (2002)
49. M.O. Ruault, J. Chaumont, J.M. Penisson, A. Bourret, *Phil. Mag. A* **50**(5), 667 (1984)
50. B.L. Eyre, *J. Phys. F: Metal Phys.* **3**, 422 (1973)
51. J. Silcox, P.B. Hirsch, *Phil. Mag.* **4**, 1356 (1959)
52. K. Kitagawa, K. Yamakawa, H. Fukushima, T. Yoshiie, Y. Hayashi, H. Yoshida, Y. Shimomura, M. Kiritani, *J. Nucl. Mater.* **133&134**, 395 (1985)
53. A. Kimura-Hashimoto, K. Suenaga, A. Gloter, K. Urita, S. Iijima, *Nature* **430**(7002), 870 (2004)
54. M. Ghaly, R.S. Averback, *Phys. Rev. Lett.* **72**(3), 364 (1994)
55. R.C. Birtcher, S.E. Donnelly, *Nucl. Instr. Meth. Phys. Res. B* **148**, 194 (1999)
56. J. Erlebacher, M.J. Aziz, E. Chason, M.B. Sinclair, J.A. Floro, *Phys. Rev. Lett.* **82**(11), 2330 (1999)
57. S.A. Norris, J. Samela, C.S. Madi, M.P. Brenner, L. Bukonte, M. Backman, F. Djurabekova, K. Nordlund, M.J. Aziz, *Nature communications* **2**, 276 (2011)
58. K. Laaziri, S. Kycia, S. Roorda, M. Chicoine, J.L. Robertson, J. Wang, S.C. Moss, *Phys. Rev. B* **60**(19), 13520 (1999)
59. S. Roorda, R.A. Hakvoort, V.A. van, P.A. Stolk, F.W. Saris, *J. Appl. Phys.* **72**(11), 5145 (1992)
60. D.C. Wallace, *Thermodynamics of crystals* (Dover, Mineola, NY, USA, 1972)
61. G.D. Watkins, in *Defects and Diffusion in Silicon Processing, MRS Symposium Proceedings*, vol. 469, ed. by T. Diaz de la Rubia, S. Coffa, P.A. Stolk, C.S. Rafferty (Materials Research Society, Pittsburgh, 1997), p. 139
62. A. Claverie, B. Colombeau, B. de Mauduit, C. Bonafos, X. Hebras, G.B. Assayag, F. Cristiano, *Appl. Phys. A* **76**, 1025 (2003)

63. F. Cristiano, N. Cherkasin, X. Hebras, P. Calvo, Y. Lamrani, E. Scheid, B. de Mauduit, B. Colombeau, W. Lerch, S. Paul, A. Claverie, Nucl. Instr. Meth. Phys. Res. B **216**, 46 (2004)
64. P. Ehrhart, (Springer, Berlin, 1991), chap. 2, p. 88
65. M. Guinan, J. Nucl. Mater. **53**, 171 (1974)
66. K.L. Merkle, W. Jäger, Phil. Mag. A **44**, 741 (1981)
67. W. Jäger, K.L. Merkle, Phil. Mag. A **57**(3), 479 (1988)
68. H.M. Urbassek, K.T. Waldeer, Phys. Rev. Lett. **67**(1), 105 (1991)
69. R.P. Webb, D.E. Harrison, Jr., Nucl. Instr. Meth. Phys. Res. **218**, 697 (1983)
70. R.C. Birtcher, S.E. Donnelly, Phys. Rev. Lett. **77**(21), 4374 (1996)
71. A. Wucher, B.J. Garrison, J. Chem. Phys. **105**(14), 5999 (1996)
72. M. Morgenstern, T. Michely, G. Comsa, Phil. Mag. A **79**(4), 775 (1999)
73. K. Nordlund, J. Keinonen, M. Ghaly, R.S. Averback, Nature **398**(6722), 49 (1999)
74. K. Kyuno, D.C. Cahill, R.S. Averback, J. Tarus, K. Nordlund, Phys. Rev. Lett. **83**, 4788 (1999)
75. C. Busse, H. Hansen, U. Linke, T. Michely, Phys. Rev. Lett. **85**, 326 (2000)
76. A.V. Krasheninnikov, Y. Miyamoto, D. Tománek, Phys. Rev. Lett. **99**, 016104 (2007)
77. Y. Miyamoto, H. Zhang, Phys. Rev. B **77**, 161402 (2008)
78. T. Kunert, R. Schmidt, Phys. Rev. Lett. **86**, 5258 (2001)
79. J.M. Pruneda, D. Sánchez-Portal, A. Arnau, J.I. Juaristi, E. Artacho, Phys. Rev. Lett. **99**, 235501 (2007). DOI 10.1103/PhysRevLett.99.235501
80. J.M. Sole, E. Artacho, J.D. Gale, A. Garcia, J. Junquera, P. Ordejón, D. Sánchez-Portal, J. Phys.: Condens. Matter **14**, 2745 (2002)
81. Y. Miyamoto, S. Berber, M. Yoon, A. Rubio, D. Tománek, Chem. Phys. Lett. **392**, 209 (2004)
82. Y. Miyamoto, A. Rubio, D. Tománek, Phys. Rev. Lett. **97**, 126104 (2006)
83. K. Eder, D. Semrad, P. Bauer, R. Golser, P. Maier-Komor, F. Aumayr, M. Peñalba, A. Arnau, J. Ugalde, P. Echenique, Phys. Rev. Lett. **79**, 4112 (1997)
84. J.I. Juaristi, C. Auth, H. Winter, A. Arnau, K. Eder, D. Semrad, F. Aumayr, P. Bauer, P. Echenique, Phys. Rev. Lett. **84**(10), 2124 (2000)
85. M. Draxler, S.P. Chenakin, S.N. Markin, P. Bauer, Phys. Rev. Lett. **95**, 113201 (2005). DOI 10.1103/PhysRevLett.95.113201. URL <http://link.aps.org/doi/10.1103/PhysRevLett.95.113201>
86. S.N. Markin, D. Primetzhofner, P. Bauer, Physical Review Letters **103**(11), 113201 (2009)
87. L.N. Serkovic Loli, E.A. Sanchez, O. Grizzi, N.R. Arista, Physical Review A **81**(2), 022902 (2010). DOI 10.1103/PhysRevA.81.022902
88. R. Martin, *Electronic structure* (Cambridge University Press, Cambridge, UK, 2004)
89. D. Porezag, T. Frauenheim, T. Köhler, G. Seifert, R. Kaschner, Phys. Rev. B **51**, 12947 (1995)
90. M. Elstner, D. Porezag, G. Jungnickel, J. Elsner, M. Haugk, T. Frauenheim, S. Suhai, G. Seifert, Phys. Rev. B **58**, 7260 (1998)
91. A.V. Krasheninnikov, F. Banhart, J.X. Li, A.S. Foster, R. Nieminen, Phys. Rev. B **72**, 125428 (2005)
92. F. Banhart, J.X. Li, A.V. Krasheninnikov, Phys. Rev. B **71**, 241408(R) (2005)
93. T. Loponen, A.V. Krasheninnikov, M. Kaukonen, R.M. Nieminen, Phys. Rev. B **74**, 073409 (2006)
94. A. Zobelli, A. Gloter, C.P. Ewels, G. Seifert, C. Colliex, Phys. Rev. B **75**, 245402 (2007)
95. Z. Wang, F. Gao, J. Li, X. Zu, W.J. Weber, Nanotechnology **20**, 075708 (2009)
96. C. Xu, C. Wang, C. Chan, K. Ho, J. Phys.: Condens. Matter **4**, 6047 (1992)
97. M. Terrones, H. Terrones, F. Banhart, J.C. Charlier, P.M. Ajayan, Science **288**, 1226 (2000)
98. M. Terrones, F. Banhart, N. Grobert, J.C. Charlier, H. Terrones, P.M. Ajayan, Phys. Rev. Lett **89**, 075505 (2002)
99. M. Terrones, P.M. Ajayan, F. Banhart, X. Blase, D.L. Carroll, J.C. Charlier, R. Czerw, B. Foley, N. Grobert, R. Kamalakaran, P. Kohler-Redlich, M. Ruhle, T. Seeger, H. Terrones, Appl. Phys. A (Materials-Science-Processing) **65**, 355 (2002)

100. F. Tran, P. Blaha, Physical Review Letters **102**(22) (2009)
101. P. Rinke, A. Janotti, M. Scheffler, C.G. Van de Walle, Physical Review Letters **102**, 026402 (2009)
102. V. Anisimov, F. Aryasetiawan, A. Lichtenstein, J. Physics-Condensed Matter **9**(4), 767 (1997)
103. M. Ernzerhof, G. Scuseria, J. Chem. Phys. **110**(11), 5029 (1999)
104. J. Heyd, G. Scuseria, M. Ernzerhof, J. Chem. Phys. **118**(18), 8207 (2003)
105. T. Korhonen, M.J. Puska, R.M. Nieminen, Phys. Rev. B **51**(15), 9526 (1996)
106. K. Carling, G. Wahnström, T.R. Mattsson, N. Sandberg, G. Grimvall, Phys. Rev. B **67**, 054101 (2003)
107. C.C. Fu, F. Willaime, P. Ordejon, Phys. Rev. Lett. **92**(17), 175503 (2004)
108. P.A. Korzhavii, A.V. Ruban, A.Y. Lozovoi, Y.K. Vekilov, I.A. Abrikosov, B. Johansson, Phys. Rev. B **61**(9), 6003 (2000)
109. Y. Mishin, A.Y. Lozovoi, A. Alavi, Phys. Rev. B **67**, 014201 (2003)
110. P. Olsson, I. Abrikosov, L. Vitos, J. Wallenius, J. Nucl. Mater. **321**, 84 (2003)
111. M.J. Puska, S. Pöykkö, M. Pesola, R.M. Nieminen, Phys. Rev. B **58**, 1318 (1998)
112. E. Holmström, A. Kuronen, K. Nordlund, Phys. Rev. B **78**(4), 045202 (2008)
113. E. Holmström, M. Hakala, K. Nordlund, Phys. Rev. B **82**, 094102 (2010)
114. T. Mattila, R.M. Nieminen, Phys. Rev. Lett. **74**, 2721 (1995)
115. S. Kuisma, K. Saarinen, P. Hautajarvi, C. Corbel, Phys. Rev. B **55**(15), 9609 (1997)
116. P. Erhart, K. Albe, A. Klein, Phys. Rev. B (2006)
117. A. Janotti, C.G. Van de Walle, Phys. Rev. B **76**(16) (2007)
118. F. Gupta, G. Brillant, A. Pasturel, Phil. Mag. **87**(16-17), 2561 (2007)
119. C.P. Ewels, R.H. Telling, A.A. El-Barbary, M.I. Heggie, P.R. Briddon, Phys. Rev. Lett. **91**, 025505 (2003)
120. A.S. Barnard, M.L. Terranova, M. Rossi, Chem. Mater. **17**, 527 (2005)
121. J.M. Carlsson, Phys. Status. Solidi (b) **243**, 3452 (2006)
122. Y. Gan, J. Kotakoski, A.V. Krasheninnikov, K. Nordlund, F. Banhart, New J. Phys. **10**, 023022 (2008)
123. P.O. Lehtinen, A.S. Foster, A. Ayuela, A. Krasheninnikov, K. Nordlund, R.M. Nieminen, Phys. Rev. Lett. **91**, 017202 (2003)
124. J.C. Meyer, F. Eder, S. Kurasch, V. Skakalova, J. Kotakoski, H.J. Park, S. Roth, A. Chuvilin, S. Eyhusen, G. Benner, A.V. Krasheninnikov, U. Kaiser, Phys. Rev. Lett. **108**, 196102 (2012)
125. M.P. López-Sancho, F. de Juan, M.A.H. Vozmediano, Phys. Rev. B **79**, 075413 (2009)
126. Y. Li, Z. Zhou, D. Golberg, Y. Bando, P.v.R. Schleyer, Z. Chen, J. Physical Chemistry C **112**(5), 1365 (2008)
127. H.P. Komsa, S. Kurasch, O. Lehtinen, U. Kaiser, A.V. Krasheninnikov, Phys. Rev. Lett. **109**, 035503 (2012)
128. H.P. Komsa, S. Kurasch, O. Lehtinen, U. Kaiser, A.V. Krasheninnikov, Phys. Rev. B **88**, 035301 (2013)
129. H.H. Andersen, Appl. Phys. **18**, 131 (1979)
130. M.P. Allen, D.J. Tildesley, *Computer Simulation of Liquids* (Oxford University Press, Oxford, England, 1989)
131. R. Lesar, *Introduction to Computational Materials Science* (Cambridge University Press, 2013)
132. W. Windl, T.J. Lenosky, J.D. Kress, A.F. Voter, Nucl. Instr. and Meth. B **141**, 61 (1998)
133. M. Tang, L. Colombo, J. Zhu, T. Diaz de la Rubia, Phys. Rev. B **55**(21), 14279 (1997)
134. F. Cargnoni, C. Gatti, L. Colombo, Phys. Rev. B **57**, 170 (1998)
135. S. Goedecker, T. Deutsch, L. Billard, Phys. Rev. Lett. **88**, 235501 (2002)
136. J. Kotakoski, J.C. Meyer, S. Kurasch, D. Santos-Cottin, U. Kaiser, A.V. Krasheninnikov, Phys. Rev. B **83**(24), 245420 (2011)
137. J. Kotakoski, C.H. Jin, O. Lehtinen, K. Suenaga, A.V. Krasheninnikov, Phys. Rev. B **82**(11), 113404 (2010)
138. F. Gao, H. Xiao, W. Weber, Nucl. Instr. Meth. Phys. Res. B **269**(14), 1693 (2011). DOI 10.1016/j.nimb.2011.01.131. URL <http://www.sciencedirect.com/science/article/pii/S0168583X11001649>

139. J. Nord, K. Nordlund, J. Keinonen, Phys. Rev. B **65**, 165329 (2002)
140. J. Nord, K. Nordlund, J. Keinonen, K. Albe, Nucl. Instr. Meth. Phys. Res. B **202**, 93 (2003)
141. M.T. Robinson, O.S. Oen, Appl. Phys. Lett. **2**(4), 30 (1963)
142. M.T. Robinson, I.M. Torrens, Phys. Rev. B **9**(12), 5008 (1974)
143. O.S. Oen, M.T. Robinson, Appl. Phys. Lett. **2**(4), 83 (1963)
144. J.F. Ziegler. SRIM-2013 software package, available online at <http://www.srim.org>.
145. J.F. Ziegler, J.P. Biersack, M.D. Ziegler, *SRIM - The Stopping and Range of Ions in Matter* (SRIM Co., Chester, Maryland, USA, 2008)
146. M.T. Robinson, Nucl. Instr. Meth. Phys. Res. B **67**, 396 (1992)
147. M. Posselt, J.P. Biersack, Nucl. Instr. Meth. Phys. Res. B **64**, 706 (1992)
148. R. Stoller, M.B. Toloczko, G.S. Was, A.G. Certain, S. Dwaraknath, F. Garner, Nucl. Instr. Meth. Phys. Res. B **310**, 75 (2013)
149. J. Likonen, M. Hautala, J. Phys.: Condens. Matter **1**, 4697 (1989)
150. K.O.E. Henriksson, K. Vörtler, S. Dreißigacker, K. Nordlund, J. Keinonen, Surf. Sci. **600**, 3167 (2006)
151. W. Möller, Nucl. Instr. Meth. Phys. Res. B **15**, 688 (1986)
152. M. Mayer, W. Eckstein, Nucl. Instr. Meth. Phys. Res. B **94**, 22 (1994)
153. R.G. Vichev, D.S. Karpuzov, Nucl. Instr. Meth. Phys. Res. B **83**, 345 (1993)
154. K. Gärtner *et al.*, Nucl. Instr. Meth. Phys. Res. B **102**(1-4), 183 (1995)
155. T.S. Pugacheva, F.G. Djurabekova, S.K. Valiev, Nucl. Instr. Meth. Phys. Res. B **141**, 99 (1998)
156. G. Hobler, D. Kovac, Nucl. Instr. Meth. Phys. Res. B **269**(14), 1609 (2011)
157. L. Bukonte, F. Djurabekova, J. Samela, K. Nordlund, S.A. Norris, M.J. Aziz, Nucl. Instr. Meth. Phys. Res. B **297**, 23 (2013)
158. J.A.V. Pomoell, A.V. Krasheninnikov, K. Nordlund, J. Keinonen, J. Appl. Phys. **96**, 2864 (2004)
159. F. Djurabekova, M. Backman, K. Nordlund, Nucl. Instr. Meth. Phys. Res. B **266**, 2683 (2008). DOI 10.1016/j.nimb.2008.03.099
160. F. Djurabekova, K. Nordlund, Phys. Rev. B **77**, 115325 (2008). Also selected to Virtual Journal of Nanoscale Science & Technology Vol. 17 Issue 13 (2008).
161. D.S. Karpuzov, V.E. Yurasova, Phys. Stat. Sol. **47**, 41 (1971)
162. K. Nordlund, Comput. Mater. Sci. **3**, 448 (1995)
163. K.M. Beardmore, N. Grønbech-Jensen, Phys. Rev. E **57**, 7278 (1998)
164. G. Hobler, G. Betz, Nucl. Instr. Meth. Phys. Res. B **180**, 203 (2001)
165. M. Posselt, Materials Science in Semiconductor Processing **3**(4), 317 (2000)
166. M. Backman, F. Djurabekova, O.H. Pakarinen, K. Nordlund, Y. Zhang, M. Toulemonde, W.J. Weber, J. Phys. D: Appl. Phys. **45**, 505305 (2012)
167. M. Backman, M. Toulemonde, O.H. Pakarinen, N. Juslin, F. Djurabekova, K. Nordlund, A. Debelle, W.J. Weber, Comput. Mater. Sci. **67**, 261 (2013)
168. M.J. Norgett, M.T. Robinson, I.M. Torrens, Nucl. Engr. and Design **33**(1), 50 (1975)
169. H.L. Heinisch, Rad. Eff. & Def. in Sol **113**, 53 (1990)
170. K. Nordlund, F. Gao, Appl. Phys. Lett. **74**(18), 2720 (1999)
171. L.A. Marqués, L. Pelaz, P. Lopez, M. Aboy, I. Santos, J. Barbolla, Mater. Sci. Engr. B **124-125**, 72 (2005)
172. I. Santos, L.A. Marqués, L. Pelaz, P. López, Nuclear Instruments and Methods in Physics Research Section B: Beam Interactions with Materials and Atoms **255**(1), 110 (2007). DOI 10.1016/j.nimb.2006.11.034. URL <http://www.sciencedirect.com/science/article/pii/S0168583X06010755>
173. I. Santos, L.A. Marqués, L. Pelaz, P. López, J. Appl. Phys. **105**(8), 083530 (2009)
174. V. Springel, Monthly notices of the royal astronomical society **364**(4), 1105 (2005)
175. E. Zarkadoula, M.T. Dove, K. Trachenko, S.L. Daraszewicz, D.M. Duffy, M. Seaton, I.T. Todorov, K. Nordlund, J. Phys. Condens. Matt. **25**(12), 125402 (2013)
176. H. Zhu, R.S. Averback, Nucl. Instr. Meth. Phys. Res. B **83**, 334 (1993)
177. W.H. Press, S.A. Teukolsky, W.T. Vetterling, B.P. Flannery, *Numerical Recipes in C; The Art of Scientific Computing*, 2nd edn. (Cambridge University Press, New York, 1995)
178. A.R. Leach, *Molecular modelling: principles and applications*, 2nd edn. (Pearson Education, Harlow, England, 2001)

179. D.W. Brenner, *Phys. Rev. B* **42**(15), 9458 (1990)
180. D.W. Brenner, O.A. Shenderova, J.A. Harrison, S.J. Stuart, B. Ni, S.B. Sinnott, *J. Phys.: Condens. Matter* **14**, 783 (2002)
181. S.J. Stuart, A.B. Tutein, J.A. Harrison, *J. Chem. Phys.* **112**(14), 6472 (2000)
182. A.C.T. van Duin, S. Dasgupta, F. Lorant, W.A.G. III, *J. Phys. Chem. A* **105**, 9396 (2001)
183. M.W. Finnis, J.E. Sinclair, *Phil. Mag. A* **50**(1), 45 (1984). *see also Erratum, ibid.* **53** (1986) 161
184. M.S. Daw, S.M. Foiles, M.I. Baskes, *Mat. Sci. Rep.* **9**, 251 (1993)
185. C.L. Kelchner, D.M. Halstead, L.S. Perkins, N.M. Wallace, A.E. DePristo, *Surf. Sci.* **310**, 425 (1994). And references therein
186. F. Cleri, V. Rosato, *Phys. Rev. B* **48**(1), 22 (1993)
187. S.L. Dudarev, P.M. Derlet, *J. Phys.: Condens. Matter* **17**, 1 (2005)
188. J. Tersoff, *Phys. Rev. B* **37**, 6991 (1988)
189. K. Albe, K. Nordlund, J. Nord, A. Kuronen, *Phys. Rev. B* **66**, 035205 (2002)
190. K. Albe, K. Nordlund, R.S. Averback, *Phys. Rev. B* **65**, 195124 (2002)
191. P. Erhart, N. Juslin, O. Goy, K. Nordlund, R. Muller, K. Albe, *J. Phys.: Condens. Matter* **18**, 6585 (2006)
192. J. Nord, K. Albe, P. Erhart, K. Nordlund, *Journal of Physics: Condensed Matter* **15**(32), 5649 (2003)
193. N. Juslin, P. Erhart, P. Träskelin, J. Nord, K.O.E. Henriksson, K. Nordlund, E. Salonen, K. Albe, *J. Appl. Phys.* **98**, 123520 (2005)
194. K.O.E. Henriksson, K. Nordlund, *Phys. Rev. B* **79**, 144107 (2009)
195. B.J. Alder, T.E. Wainwright, (Wiley Interscience, New York, 1957), *Proc. Intern. Symposium on Transport Processes in Statistical Mechanics*, p. 97
196. H. Andersen, *J. Chem. Phys.* **72**(4), 2384 (1980). DOI 10.1063/1.439486
197. W. Still, A. Tempczyk, R. Hawley, T. Hendrickson, *J. Amer. Chem. Soc.* **112**(16), 6127 (1990). DOI 10.1021/ja00172a038
198. S.L. Mayo, B.D. Olafson, W.A.G. III, *J. Phys. Chem.* **94**, 8897 (1990)
199. A. Rappe, C. Casewit, K. Colwell, W. Goddard, W. Skiff, *J. Amer. Chem. Soc.* **114**(25), 10024 (1992). DOI 10.1021/ja00051a040
200. S. Plimpton, *J. Comput. Physics* **117**(1), 1 (1995). DOI 10.1006/jcph.1995.1039
201. A. MacKerell, D. Bashford, M. Bellott, R. Dunbrack, J. Evanseck, M. Field, S. Fischer, J. Gao, H. Guo, S. Ha, D. Joseph-McCarthy, L. Kuchnir, K. Kuczera, F. Lau, C. Mattos, S. Michnick, T. Ngo, D. Nguyen, B. Prodhom, W. Reiher, B. Roux, M. Schlenkrich, J. Smith, R. Stote, J. Straub, M. Watanabe, J. Wiorkiewicz-Kuczera, D. Yin, M. Karplus, *J. Phys. Chem. B* **102**(18), 3586 (1998)
202. D. Van der Spoel, E. Lindahl, B. Hess, G. Groenhof, A. Mark, H. Berendsen, *J. Comput. Chem.* **26**(16), 1701 (2005). DOI 10.1002/jcc.20291
203. K. Nordlund, M. Ghaly, R.S. Averback, M. Caturla, T. Diaz de la Rubia, J. Tarus, *Phys. Rev. B* **57**(13), 7556 (1998)
204. J.B. Gibson, A.N. Goland, M. Milgram, G.H. Vineyard, *Phys. Rev.* **120**(4), 1229 (1960)
205. C. Erginsoy, G.H. Vineyard, A. Englert, *Phys. Rev.* **133**(2), A595 (1964)
206. R.P. Webb, D.E. Harrison, Jr., *Phys. Rev. Lett.* **50**, 1478 (1983)
207. B.D. Wirth, G.R. Odette, D. Maroudas, G.E. Lucas, *J. Nuclear Materials* **244**(3), 185 (1997)
208. T. Diaz de la Rubia, G.H. Gilmer, *Phys. Rev. Lett.* **74**(13), 2507 (1995)
209. W.J. Phythian, R.E. Stoller, A.J.E. Foreman, A.F. Calder, D.J. Bacon, *J. Nucl. Mater.* **223**, 245 (1995)
210. M. Kerford, R.P. Webb, *Nucl. Instr. Meth. Phys. Res. B* **140**, 44 (2001)
211. C. Schäfer, H.M. Urbassek, L.V. Zhigilei, *Phys. Rev. B* **66**, 115404 (2002)
212. A. Delcorte, X.V. Eynde, P. Bertrand, J.C. Vickerman, B.J. Garrison, *J. Phys. Chem.* **104**, 2673 (2000)
213. Z. Postawa, B. Czerwinski, M. Szewczyk, E.J. Smiley, N. Winograd, B.J. Garrison, *Anal. Chem.* **75**, 4402 (2003)
214. D. Terentyev, L. Malerba, R. Chakarova, C. Domain, K. Nordlund, P. Olsson, M. Rieth, J. Wallenius, *J. Nucl. Mater.* **249**, 119 (2006)
215. A. Duvenbeck, B. Weidtmann, O. Weingart, A. Wucher, *Phys. Rev. B* **77**, 245444 (2008)

216. O. Lehtinen, J. Kotakoski, A.V. Krasheninnikov, A. Tolvanen, K. Nordlund, J. Keinonen, *Phys. Rev. B* **81**, 153401 (2010)
217. J. Polvi, P. Luukkonen, K. Nordlund, T.T. Järvi, T.W. Kemper, S.B. Sinnott, *J. Phys. Chem. B* **116**(47), 13932 (2012)
218. J.A. Brinkman, *J. Appl. Phys.* **25**, 961 (1954)
219. R. Devanathan, W.J. Weber, T. Diaz de la Rubia, *Nucl. Instr. Meth. Phys. Res. B* **141**(14), 118 (1998)
220. C. Björkas, K. Vörtler, K. Nordlund, *Phys. Rev. B (Rapid comm.)* **74**, 140103 (2006)
221. T.T. Järvi, J.A. Pakarinen, A. Kuronen, K. Nordlund, *EPL* **82**, 26002 (2008)
222. S. Hoilijoki, E. Holmström, K. Nordlund, *J. Appl. Phys.* **110**(4), 043540 (2011)
223. W. Ren, A. Kuronen, K. Nordlund, *Phys. Rev. B* **86**, 104114 (2012)
224. G. Greaves, J.A. Hinks, P. Busby, N.J. Mellors, A. Ilinov, A. Kuronen, K. Nordlund, S.E. Donnelly, *Phys. Rev. Lett.* **111**, 065504 (2013)
225. J. Nord, K. Nordlund, J. Keinonen, *Phys. Rev. B* **68**, 184104 (2003)
226. J. Kotakoski, A.V. Krasheninnikov, K. Nordlund, *Phys. Rev. B* **74**(24), 245420 (2006)
227. A.V. Krasheninnikov, K. Nordlund, M. Sirviö, E. Salonen, J. Keinonen, *Phys. Rev. B* **63**, 245405 (2001)
228. A.V. Krasheninnikov, K. Nordlund, J. Keinonen, *Phys. Rev. B* **65**, 165423 (2002). Also selected to *Virtual Journal of Nanoscale Science & Technology* Vol. 5 Issue 16 (2002).
229. A.V. Krasheninnikov, *Sol. Stat. Comm.* **118**, 361 (2001)
230. A.V. Krasheninnikov, K. Nordlund, *J. Vac. Sci. Techn. B* **20**(2), 728 (2001)
231. A.V. Krasheninnikov, K. Nordlund, J. Keinonen, F. Banhart, *Phys. Rev. B* **66**, 245403 (2002)
232. M. Sammalkorpi, A.V. Krasheninnikov, A. Kuronen, K. Nordlund, K. Kaski, *Nucl. Instr. Meth. Phys. Res. B* **228**, 142 (2005)
233. A.V. Krasheninnikov, K. Nordlund, J. Keinonen, *Appl. Phys. Lett.* **81**, 1101 (2002). Also selected to *Virtual Journal of Nanoscale Science & Technology* Vol. 6 Issue 7 (2002).
234. L. Sun, F. Banhart, A.V. Krasheninnikov, J.A. Rodriguez-Manzo, M. Terrones, P.M. Ajayan, *Science* **312**, 1199 (2006)
235. L. Sun, A.V. Krasheninnikov, T. Ahlgren, K. Nordlund, F. Banhart, *Phys. Rev. Lett.* **101**, 156101 (2008). See also commentary on article by S. Suresh and J. Li, *Nature* 456 (2008) 717.
236. A. Meftah, F. Brisard, J.M. Costantini, E. Dooryhee, M. Hage-Ali, M. Hervieu, J.P. Stoquert, F. Studer, M. Toulemonde, *Phys. Rev. B* **49**, 12457 (1994)
237. M. Toulemonde, C. Dufour, A. Meftah, E. Paunier, *Nucl. Instr. Meth. Phys. Res. B* **166-167**, 903 (2000)
238. S. Klaumünzer, M.D. Hou, G. Schumacher, *Phys. Rev. Lett.* **57**(7), 850 (1986)
239. N.A. Medvedev, A.E. Volkov, N.S. Shcheblanov, B. Rethfeld, *Physical Review B* **82**(12) (2010)
240. N.A. Medvedev, A.E. Volkov, K. Schwartz, C. Trautmann, *Physical Review B* **87**(10) (2013)
241. E.M. Bringa, R.E. Johnson, *Phys. Rev. Lett.* **88**(16), 165501 (2002)
242. D.M. Duffy, A.M. Rutherford, *J. Phys. Cond. Matter* **19**, 016207 (2007)
243. P. Kluth, C.S. Schnohr, O.H. Pakarinen, F. Djurabekova, D.J. Sprouster, R. Giulian, M.C. Ridgway, A.P. Byrne, C. Trautmann, D.J. Cookson, K. Nordlund, M. Toulemonde, *Phys. Rev. Lett.* **101**, 175503 (2008)
244. O.H. Pakarinen, F. Djurabekova, K. Nordlund, *Nucl. Instr. Meth. Phys. Res. B* **268**, 3163 (2010)
245. E.M. Bringa, *Nucl. Instr. Meth. Phys. Res. B* **209**, 1 (2003)
246. R. Devanathan, P. Durham, J. Du, L.R. Corrales, E.M. Bringa, *Nucl. Instr. Meth. Phys. Res. B* **255**, 172 (2007)
247. J. Frantz, J. Tarus, K. Nordlund, J. Keinonen, *Phys. Rev. B* **64**, 125313 (2001)
248. A. Duvenbeck, O. Weingart, V. Buss, A. Wucher, *New J. Physics* **9**, 38 (2007)
249. M. Ridgway, T. Bierschen, R.G. , B. Afra, M.D. Rodriguez, L. Araujo, A.P. Byrne, N. Kirby, O.H. Pakarinen, F. Djurabekova, K. Nordlund, M. Schleberger, O. Osmani, N. Medvedev, B. Rethfeld, W. Wesch, P. Kluth, *Phys. Rev. Lett.* **110**, 245502 (2013)
250. O. Osmani, N. Medvedev, M. Schleberger, B. Rethfeld, *Phys. Rev. B* **84**, 214105 (2011)

251. M. Posselt, A. Gabriel, *Phys. Rev. B* **80**, 045202 (2009)
252. J. Tersoff, *Phys. Rev. B* **39**(8), 5566 (1989). ; *idem*, 41, 3248 (1990).
253. A.F. Voter, M.R. Sorensen, in *Multiscale Modelling of Materials, MRS Symp. Proc.*, vol. 538, ed. by V.V. Bulatov, T.D. de la Rubia, R. Phillips, E. Kaxiras, N. Ghoniem (Materials Research Society, Pittsburgh, 1999), p. 427
254. A.F. Voter, F. Montalenti, T.C. Germann, *Annu. Rev. Mater. Res.* **32**, 321 (2002)
255. S. Blackwell, R. Smith, S.D. Kenny, J.M. Walls, *Phys. Rev. B* **86**, 035416 (2012)
256. W.M. Young, E.W. Elcock, *Proc. Phys. Soc* **89**, 735 (1966)
257. A.B. Bortz, M.H. Kalos, J.L. Lebowitz, *J. Computational Physics* **17**, 10 (1975)
258. K.A. Fichthorn, W.H. Weinberg, *J. Chem. Phys* **95**(2), 1090 (1991)
259. J. Kotakoski, A.V. Krasheninnikov, K. Nordlund, *J. Comp. Theor. Nanosci* **4**, 1153 (2007)
260. F.G. Djurabekova, L. Malerba, C. Domain, C.S. Becquart, *Nucl. Instr. Meth. Phys. Res. B* **255**(1), 47 (2007)
261. J. Dalla Torre, J. Bocquet, N.V. Doan, E. Adam, A. Barbu, *Phil. Mag. A* **85**, 549 (2005)
262. T. Opplestrup, V.V. Bulatov, G.H. Gilmer, M.H. Kalos, B. Sadigh, *Phys. Rev. Lett.* **97**, 230602 (2006)
263. A.V. Krasheninnikov, K. Nordlund, P.O. Lehtinen, A.S. Foster, A. Ayuela, R.M. Nieminen, *Phys. Rev. B* **69**, 073402 (2004)
264. J. Kotakoski, A.V. Krasheninnikov, K. Nordlund, *J. Computat. and Theor. Nanoscience* **4**, 1153 (2007)
265. H. Jónsson, G. Mills, G.K. Schenter, *Surf. Sci.* **324**, 305 (1995)
266. J.W. Mayer, S.S. Lau, *Electronic Materials Science For Integrated Circuits in Si and GaAs* (MacMillan, New York, 1990)
267. J. Nord, K. Nordlund, J. Keinonen, *Nucl. Instr. Meth. Phys. Res. B* **193**, 294 (2002)
268. D.J. Eaglesham, P.A. Stolck, H.J. Gossmann, J.M. Poate, *Appl. Phys. Lett.* **65**, 2305 (1995)
269. S. Libertino, J.L. Benton, S. Coffa, D.C. Jacobsen, D.J. Eaglesham, J.M. Poate, M. Lavalle, P.G. Fuoichi, in *Defects and Diffusion in Silicon Processing, MRS Symposium Proceedings*, vol. 469, ed. by T. Diaz de la Rubia, S. Coffa, P.A. Stolck, C.S. Rafferty (Materials Research Society, Pittsburgh, 1997), p. 187
270. N.E.B. Cowern, G. Mannino, P.A.S.F. Roozeboom, H.G.A. Huizing, J.G.M. van Berkum, F. Cristiano, A. Claverie, M. Jaraiz, *Phys. Rev. Lett.* **82**(22), 4460 (1999)
271. L. Pelaz, L.A. Marqués, M. Aboy, J. Barbolla, G.H. Gilmer, *Appl. Phys. Lett.* **82**(13), 2038 (2003)
272. L. Pelaz, M. Jaraiz, H.H. Gilmer, H.J. Gossmann, C.S. Rafferty, D.J. Eaglesham, J.M. Poate, *Appl. Phys. Lett.* **70**(17), 2285 (1997)
273. L. Pelaz, L.A. Marqués, J. Barbolla, *J. Applied Physics* **96**(11), 5947 (2004)
274. M. Aboy, L. Pelaz, L.A. Marqués, L. Enriquez, J. Barbolla, *J. Appl. Phys.* **94**(2), 1013 (2003)
275. P. Lopez, L. Pelaz, L.A. Marqués, I. Santos, M. Aboy, J. Barbolla, *Mater. Sci. Engr. B* **114-115**, 82 (2004)
276. M. Aboy, L. Pelaz, L.A. Marqués, P. López, J. Barbolla, R. Duffy, V.C. Venezia, P.B. Griffin, *Appl. Phys. Lett.* **86**, 031908 (2005)
277. M. Aboy, L. Pelaz, E. Bruno, S. Mirabella, S. Boninelli, *J. Appl. Phys.* **110**, 073524 (2011)
278. M. Jaraiz, G.H. Gilmer, J.M. Poate, T. Diaz de la Rubia, *Appl. Phys. Lett.* **68**(3), 409 (1996)
279. M. Jaraiz, L. Pelaz, J.E. Rubio, J. Barbolla, G.H. Gilmer, D.J. Eaglesham, H.J. Gossmann, J. Poate, *Mat. Res. Soc. Symp. Proc.* **532**, 43 (1998)
280. B. Colombeau, N.E.B. Cowern, F. Cristiano, P. Calvo, N. Cherkashin, Y. Lamrani, A. Claverie, *Appl. Phys. Lett.* **83**(10), 1953 (2003)
281. P.A. Fedders, D.A. Drabold, S. Klemm, *Phys. Rev. B* **45**, 4048 (1992)
282. B.R. Djordjevic, M.F. Thorpe, F. Wooten, *Phys. Rev. B* **52**, 5685 (1995)
283. S.E. Donnelly, R.C. Birtcher, V.M. Vishnyakov, G. Carter, *Appl. Phys. Lett.* **82**, 1860 (2003)
284. F. Djurabekova, S. Parviainen, A. Pohjonen, K. Nordlund, *Phys. Rev. E* **83**(2), 026704 (2011)

-
285. S. Parviainen, F. Djurabekova, H. Timko, K. Nordlund, *Comput. Mater. Sci.* **50**(7), 2075 (2011)
286. A.S. Pohjonen, S. Parviainen, T. Muranaka, F. Djurabekova, *J. Appl. Phys.* (2013)
287. D.S. Ivanov, L.V. Zhigilei, *Phys. Rev. B* **68**, 064114 (2003)